RESIN FILM INFUSION (RFI) PROCESS MODELING FOR LARGE TRANSPORT AIRCRAFT WING STURCTURES

Grant Number NAG-1-1881 Supplement 2

Final Report

Period of Performance: December 10, 1997 - December 9, 1998

Tamara W. Knott
Alfred C. Loos

Department of Engineering Science and Mechanics
Virginia Polytechnic Institute and State University
Blacksburg, VA 24061

August 15, 2000

Prepared For:
Mr. H. Benson Dexter
NASA Langley Research Center
Hampton, VA 23681

Contents

List of Figures

List of Tables

1 Introduction

Resin film infusion (RFI) is a cost-effective method for fabricating stiffened aircraft wing structures. The RFI process lends itself to the use of near net shape textile preforms manufactured through a variety of automated textile processes such as knitting and braiding. Often, these advanced fiber architecture preforms have through-the-thickness stitching for improved damage tolerance and delamination resistance. The challenge presently facing RFI is to refine the process to ensure complete infiltration and cure of a geometrically complex shape preform with the high fiber volume fraction needed for structural applications. An accurate measurement of preform permeability is critical for successful modeling of the RFI resin infiltration process. Small changes in the permeability can result in very different infiltration behavior and times. Therfore, it is important to accurately measure the permeabilities of the textile preforms used in the RFI process. The objective of this investigation was to develop test methods that can be used to measure the compaction behavior and permeabilities of high fiber volume fraction, advanced fiber architecture textile preforms. These preforms are often highly compacted due to through-the-thickness stitching used to improve damage tolerance. Test fixtures were designed and fabricated and used to measure both transverse and in-plane permeabilities. The fixtures were used to measure the permeabilities of multiaxial warp knit and triaxial braided preforms at fiber volume fractions from 55% to 65%. In addition, the effects of stitching characteristics, thickness, and batch variability on permeability and compaction behavior were investigated.

2 Permeability

The flow model requires permeabilities of the textile preform. These data were obtained experimentally for two types of preforms, and for a bleeder material. The first type of preform is a multiaxial warp knit fabric (MAWK) that contains seven layers of unidirectional carbon fibers laid up in a quasi-isotropic stacking sequence. The seven layers are knitted together with a polyester thread, and the knitted unit is referred to as a "stack". The stack is taken to be an orthotropic material. Preforms made from three different fiber systems,

Hexcel AS4, Tenax HTA, and a Hexcel AS4/IM7 hybrid were studied. Details of the warp knit fabric can be found in [1–3]. The second type of preform is a stitched triaxial braided carbon fiber fabric. The tows are braided around a cylindrical mandrel to form a tube. The tubes were fabricated with Hexcel AS4 6k carbon fiber bias yarns at a braid angle of 60° and with IM7 36k carbon fiber axial yarns. Approximately 44% of the fibers were in the axial direction and 56% of the fibers were in the off-axis directions. The tube is flattened to form a layer. The breather material studied was a Knytex 7544 glass fiber plain weave fabric.

To construct a preform, the stacks or tubes of material are cut to the desired dimensions and stacked together. The material is then stitched through the thickness using a modified lock stitch and Kevlar thread. The preforms tested were 8-stack Tenax MAWK, 6-stack AS4 MAWK, 4-, 8-, and 16-stack AS4/IM7 MAWK, and 4-tube and 14-tube braid. The Hexcel AS4 preforms were stitched at several stitch densities. The stitch rows were spaced 0.2, 0.3, 0.5, or 0.75 inches apart, and the stitch step was 1/8 inch. The stitch density is indicated as (row spacing:stitch step) in inches. The Tenax HTA and Hexcel AS4/IM7 preforms were stitched at (0.2:1/8). The 8-stack AS4/IM7 was tested from two batches. In addition, some samples of the 8-stack AS4/IM7 were heat set prior to testing. Properties of the Knytex 7544 glass fabric were determined using 10 plys of the fabric stacked, but not stitched, together.

2.1 Permeability Measurements

There are two common methods for measuring the permeability of fabrics and preforms. These are the steady-state and advancing front measurements. The materials used in this study were characterized using steady state measurements. The steady-state method measures the permeability of a saturated preform under constant flow rate conditions, as a function of fiber volume fraction. The preform is compressed to the desired fiber volume fraction and saturated with a fluid of known viscosity. As fluid flows through the preform, the pressure drop across the preform length is measured. The fixtures used were designed to create a one-dimensional flow. The permeability of the preform is then determined from the one-dimensional form of Darcy's Law, which is written as

$$q = \frac{S\Delta P}{\mu L}, \tag{1}$$

Table 1: Test Matrix for Tenax HTA MAWK Permeability Tests

	No.of tests	Avg Areal Wt g/m^2	% Variation Areal Wt
8-stack			
$\parallel$ to stitching	3	1535	0.24
$\perp$ to stitching	3	1534	0.30
TTT	3	1487	0.50

where the superficial or filter velocity (q) is proportional to the pressure drop (ΔP) across the length (L) of a porous medium. The proportionality constants are the fluid viscosity (μ) and the experimentally determined permeability constant (S). Assuming that the material is orthotropic, permeability measurements must be made in three mutually perpendicular directions to fully characterize the preform. For stitched preforms these directions are in-plane parallel to the stitching, in-plane normal to the stitching, and transverse to the stitching (TTT) direction. With the steady-state method one preform sample is needed to determine the permeability through a range of fiber volume fractions in each of the three directions. A summary of the number of samples tested, the average areal weights of the samples and the percent variation of the sample areal weights from the average for each material are presented in Tables 1- 5.

Table 2: Test Matrix for Hexcel AS4 MAWK Permeability Tests

	No.of tests	Avg Areal Wt g/m^2	% Variation Areal Wt
6-stack (0.2:1/8)			
$\parallel$ to stitching	2	1548	0.06
$\perp$ to stitching	2	1546	0.16
TTT	2	1536	1.70
6-stack (0.3:1/8)			
$\parallel$ to stitching	2	1527	0.33
$\perp$ to stitching	2	1520	0.30
TTT	2	1500	0.67
6-stack (0.5:1/8)			
$\parallel$ to stitching	2	1511	0.20
$\perp$ to stitching	2	1513	0.20
TTT	2	1500	0.20
6-stack (0.75:1/8)			
$\parallel$ to stitching	2	1511	0.53
$\perp$ to stitching	2	1505	0.01
TTT	2	1510	0.43

The permeability measurement system is composed of a data acquisition system, permeability fixtures, and a constant flow rate pump. The real-time data acquisition and data reduction system is comprised of a National Instruments(NI) data acquisition board, NI SCXI signal conditioning and multiplexing hardware, and LabVIEW data acquisition software running on a PC. Communication with a Parker Zenith precision gear metering pump is handled through a Zenith Zetrol control unit via RS-422. A complete description of the system can be found in Fingerson, Loos, and Dexter [4].

Figure 1 shows a picture of the fixture for measuring the in-plane permeability. Fingerson, Loos, and Dexter [4] have given detailed drawings of this fixture. The mold cavity is 17.78 cm long and 15.32 cm wide, and the preform is 15.2 cm long and 15.32 cm wide. The gap between the cavity length forms an inlet manifold allowing even inlet pressure across the face of the preform.

Figure 2 is a sketch of the through-the-thickness permeability fixture set-up. A detailed description of the fixture can be found in Weideman [5] and Hammond et al. [6]. The test fixture was designed to characterize 5.1 cm long by 5.1 cm wide fabric preform samples. The

Table 3: Test Matrix for Hexcel AS4/IM7 MAWK Permeability Tests

	No.of tests	Avg Areal Wt g/m^2	% Variation Areal Wt
4-stack			
$\parallel$ to stitching	3	1519	0.26
$\perp$ to stitching	2	1520	0.19
TTT	2	1508	0.33
8-stack batch 1			
$\parallel$ to stitching	2	1524	0.0
$\perp$ to stitching	2	1521	0.03
TTT	3	1518	0.35
8-stack batch 2			
$\parallel$ to stitching	2	1512	0.46
$\perp$ to stitching	2	1511	0.73
TTT	2	1464	0.68
8-stack batch 1 heat set			
$\parallel$ to stitching	1	1505	-
$\perp$ to stitching	2	1518	0.13
TTT	2	1503	0.66
16-stack			
$\parallel$ to stitching	2	1522	0.53
$\perp$ to stitching	2	1523	0.13
TTT	3	1453	1.18

Table 4: Test Matrix for Triaxial Braid Permeability Tests

	No.of tests	Avg Areal Wt g/m^2	% Variation Areal Wt
4-Tube			
$\parallel$ to stitching	3	1259	0.20
$\perp$ to stitching	3	1261	1.00
TTT	3	1240	1.60
14-Tube			
$\parallel$ to stitching	3	1285	0.30
$\perp$ to stitching	3	1286	0.30
TTT	2	1238	0.20

Table 5: Test Matrix for Knytex 7544 Glass Fabric Permeability Tests

	No.of tests	Avg Areal Wt g/m^2	% Variation Areal Wt
Knytex 7544 Plain Weave Glass Fabric			
warp	2	633	0.08
fill	2	634	0.0
TTT	3	633	0.58

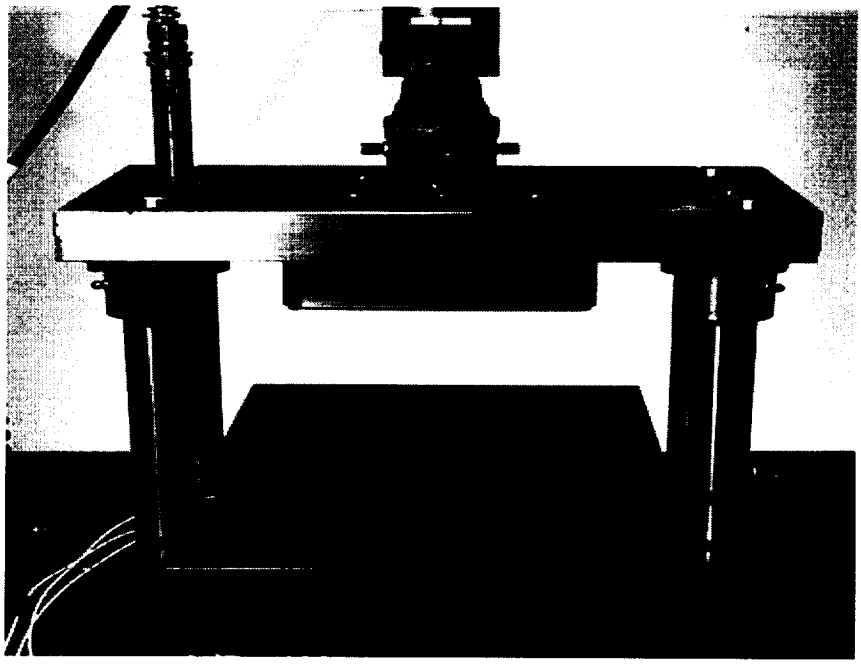

Figure 1: In-plane permeability measurement fixture.

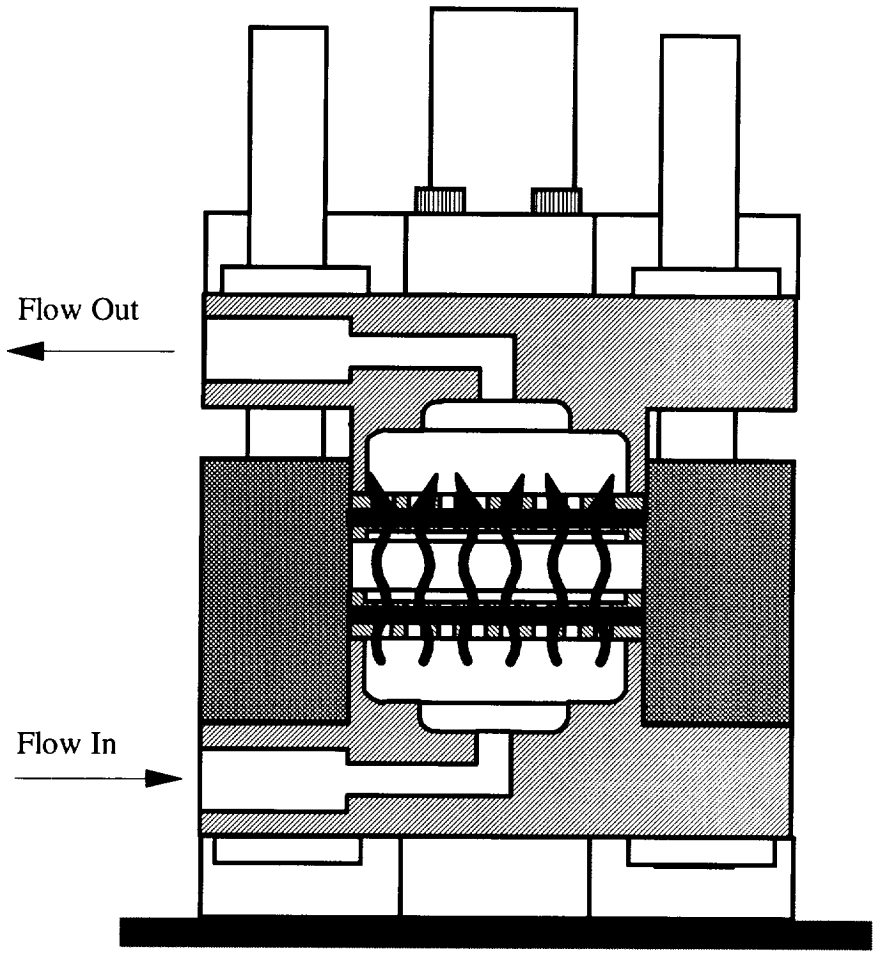

Figure 2: Through the thickness permeability measurement fixture.

upper and lower surfaces of the mold cavity compress the preform and contain holes for the fluid to flow through the thickness of the preform.

Specimens were cut out of a larger preform so that they would fit tightly in the mold. The stitched preforms were cut with a band saw and trimmed as necessary. The layers of glass were cut with a circular razor blade or exacto knife and template. To measure the permeabilities, a preform sample is placed in the test fixture and the mold is closed. Compaction pressure is applied, and the initial thickness is measured. The fluid is then pumped through the preform using the Parker Zenith precision gear metering pump. One of two fluids was used, either corn oil, with a viscosity of 0.054-0.057 Pa·s, or Mobiltherm 603, with a viscosity of 0.034-0.040 Pa·s. The flow rate is held constant until the inlet pressure reaches a steady value. The permeability and the fiber volume fraction are then recorded

Table 6: Permeability Fit Constants for Tenax HTA MAWK

	a	b
8 Stack		
$\parallel$ to stitching	9.03×10^{-15}	-12.18
$\perp$ to stitching	3.27×10^{-15}	-12.53
TTT	1.26×10^{-14}	-7.95

directly from the LabVIEW software. For the tests conducted, permeability was measured for values of fiber volume fraction between 50 and 64 percent for the graphite preforms and 45 and 60 percent for the glass fabric. The following equation was used to fit the permeability data in each direction:

$$S = a(v_f)^b \tag{2}$$

where S is the permeability in m^2, v_f is the fiber volume fraction, and a and b are fit constants. Figure 3 shows the data and power-law fit curves for the permeability parallel, normal, and transverse to the stitching as a function of fiber volume fraction for the HTA Tenax preform. Figures 4 - 7 show the permeability results for the Hexcel AS4 preforms. The permeability results for the AS4/IM7 preforms are presented in Figures 8-12. The permeability results for the braided materials are shown in Figures 13 and 14. And Figure 15 shows the permeability data and power-law fit curves for Knytex 7544 glass fabric. The fit constants for the materials tested are listed in Tables 6 - 10.

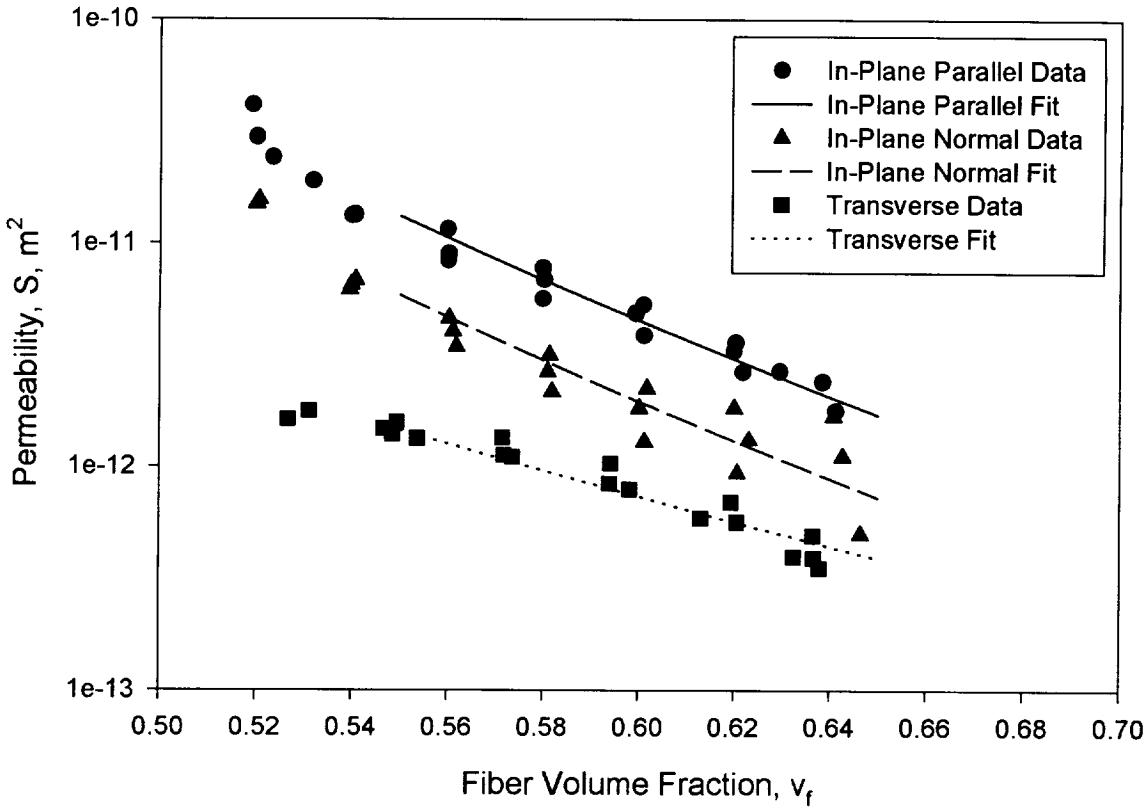

Figure 3: Permeability of Tenax HTA Multiaxial Warp Knit Fabric.

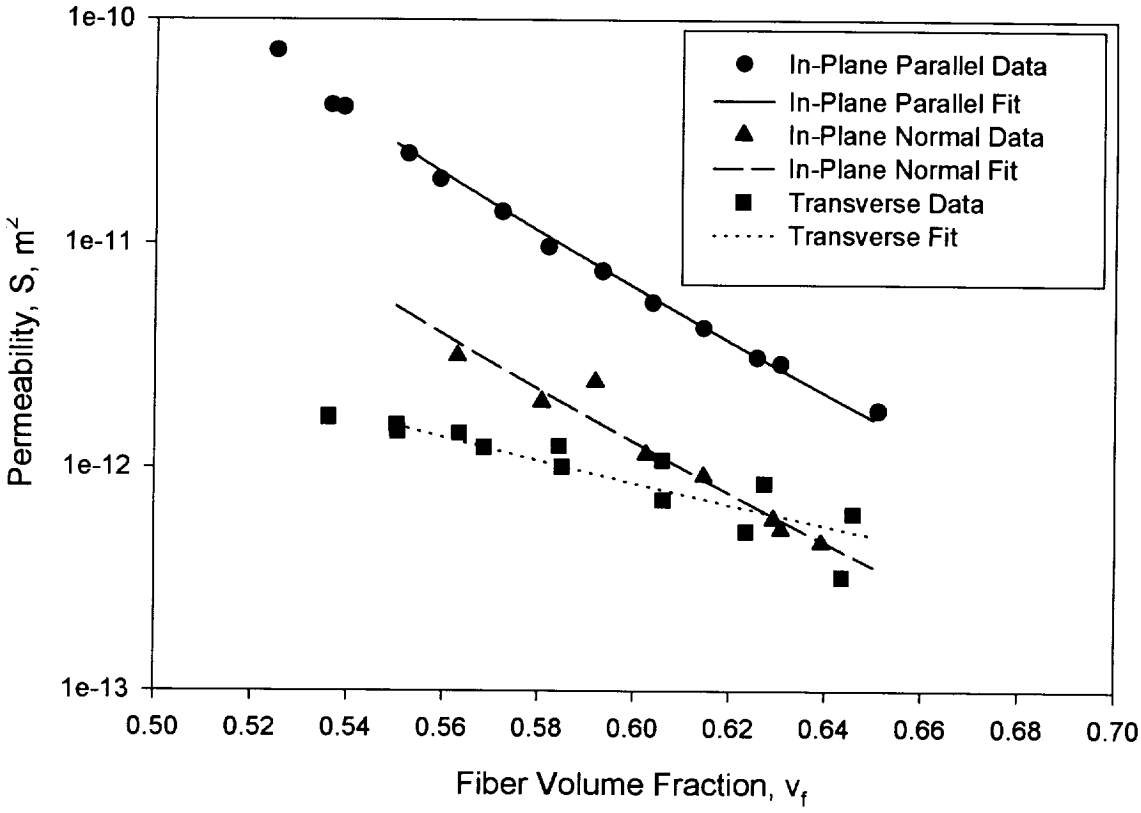

Figure 4: Permeability of Hexcel AS4 (0.2:1/8) Multiaxial Warp Knit Fabric.

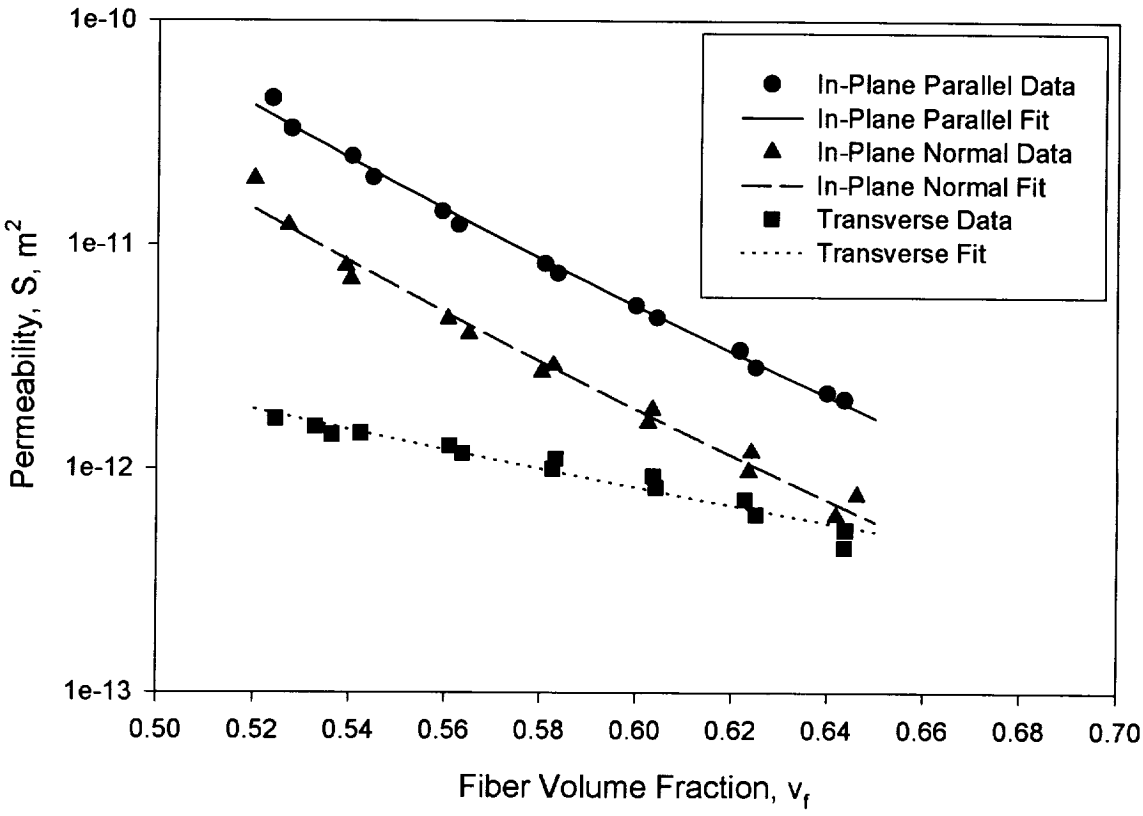

Figure 5: Permeability of Hexcel AS4 (0.3:1/8) Multiaxial Warp Knit Fabric.

Table 7: Permeability Fit Constants for Hexcel AS4 MAWK

	a	b
6-stack (0.2:1/8)		
$\parallel$ to stitching	1.13×10^{-15}	-16.91
$\perp$ to stitching	3.59×10^{-16}	-16.04
TTT	2.63×10^{-14}	-6.81
6-stack (0.3:1/8)		
$\parallel$ to stitching	3.41×10^{-15}	-14.39
$\perp$ to stitching	1.15×10^{-15}	-14.4
TTT	4.64×10^{-14}	-5.63
6-stack (0.5:1/8)		
$\parallel$ to stitching	6.25×10^{-15}	-13.39
$\perp$ to stitching	1.90×10^{-15}	-13.19
TTT	1.55×10^{-14}	-7.53
6-stack (0.75:1/8)		
$\parallel$ to stitching	1.03×10^{-14}	-12.51
$\perp$ to stitching	2.78×10^{-15}	-12.81
TTT	3.48×10^{-14}	-5.95

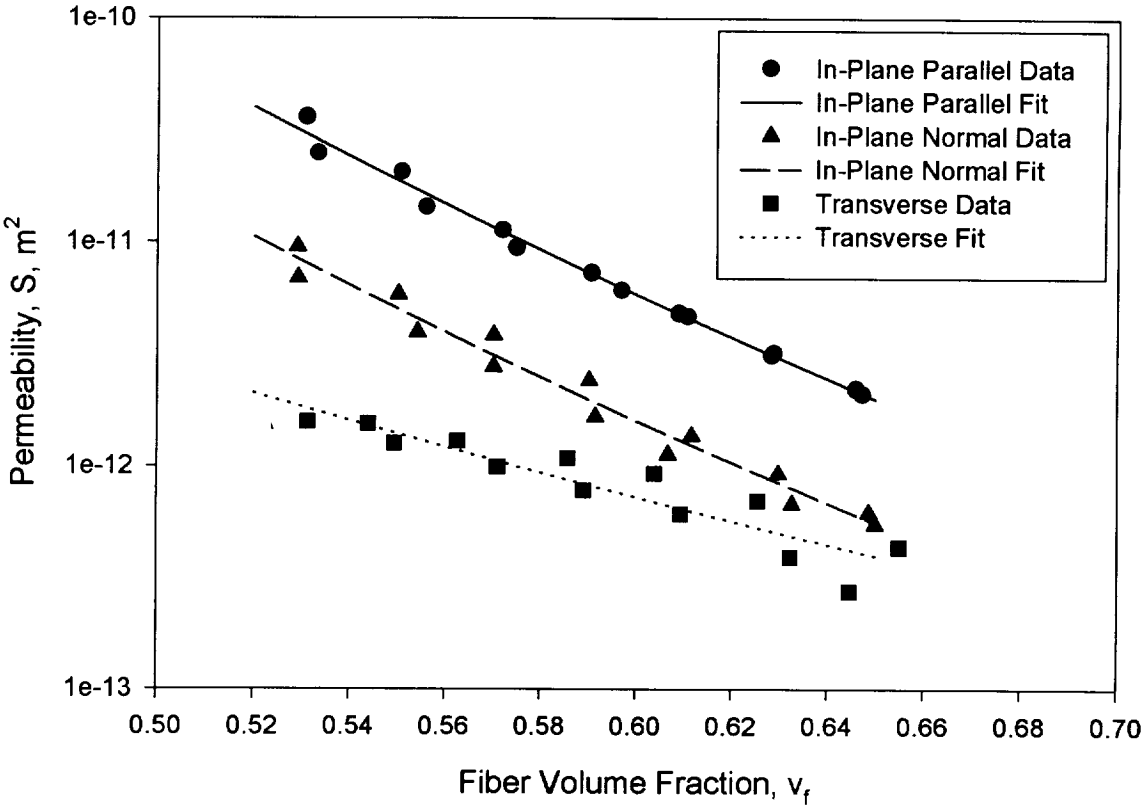

Figure 6: Permeability of Hexcel AS4 (0.5:1/8) Multiaxial Warp Knit Fabric.

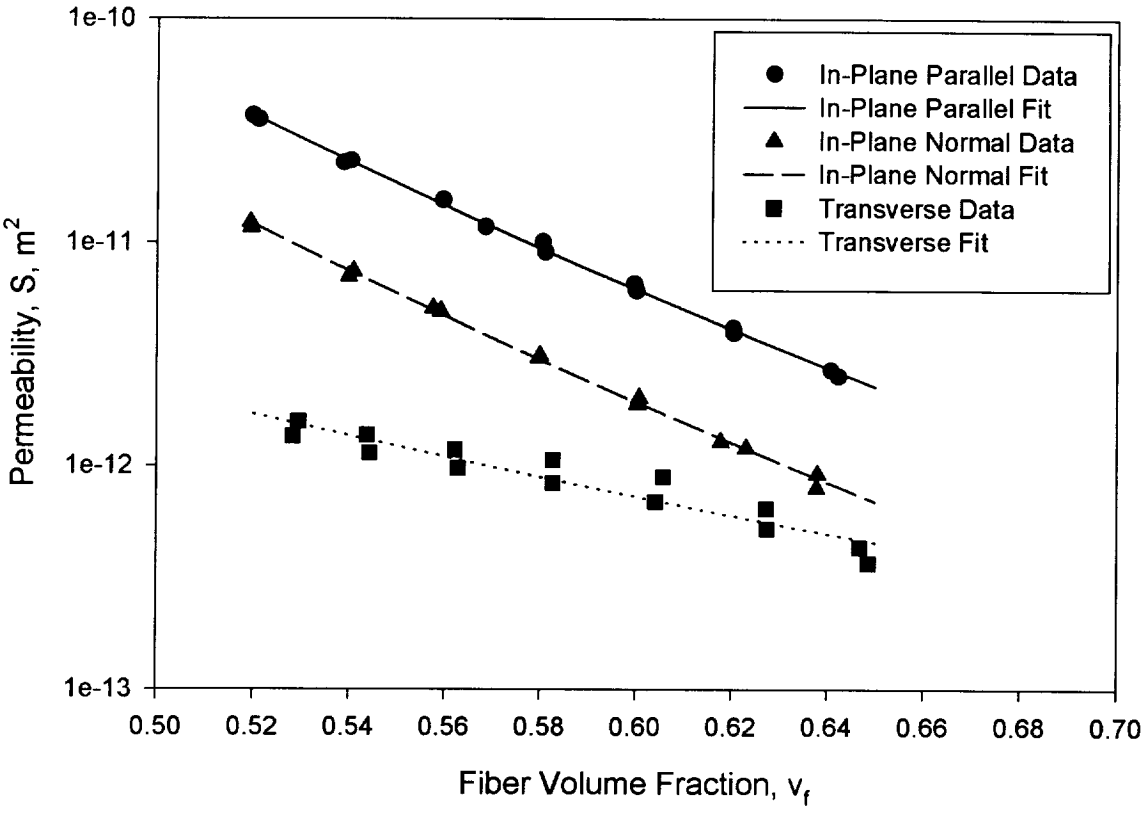

Figure 7: Permeability of Hexcel AS4 (0.75:1/8) Multiaxial Warp Knit Fabric.

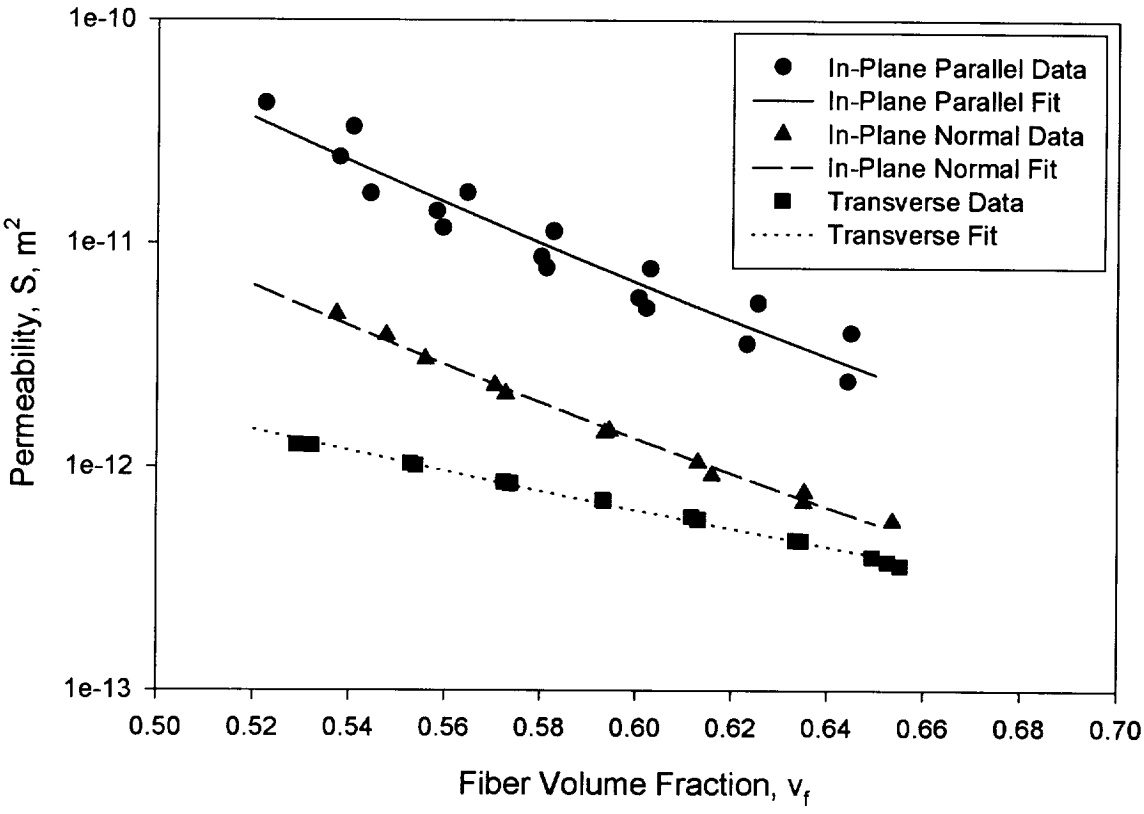

Figure 8: Permeability of Hexcel AS4/IM7 4-Stack Multiaxial Warp Knit Fabric.

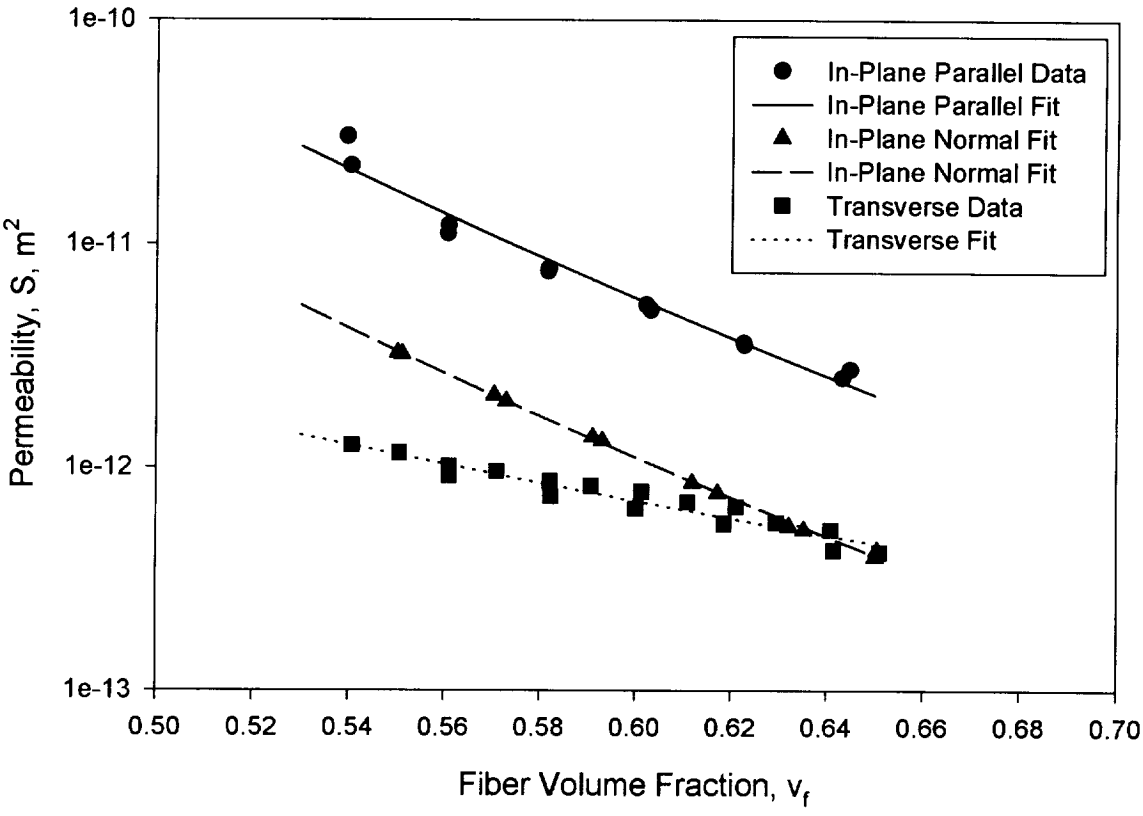

Figure 9: Permeability of Hexcel AS4/IM7 8-Stack Batch 1 Multiaxial Warp Knit Fabric.

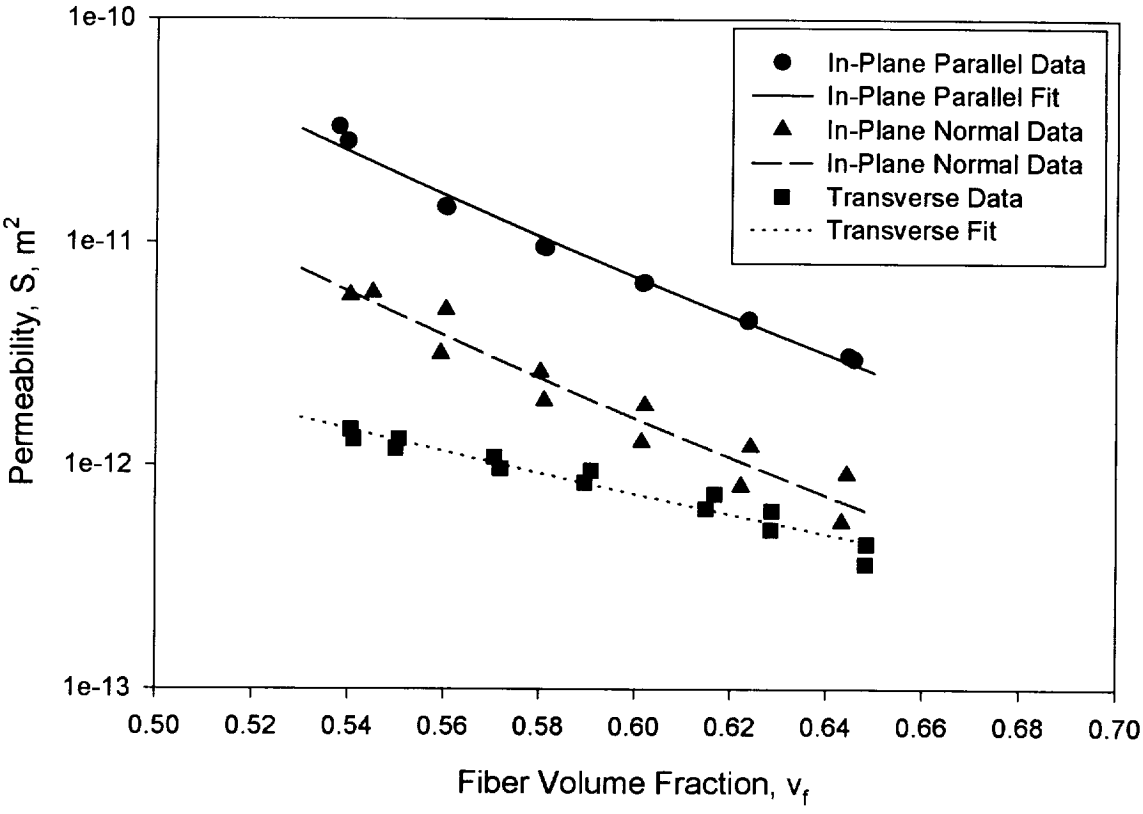

Figure 10: Permeability of Hexcel AS4/IM7 8-Stack Batch 2 Multiaxial Warp Knit Fabric.

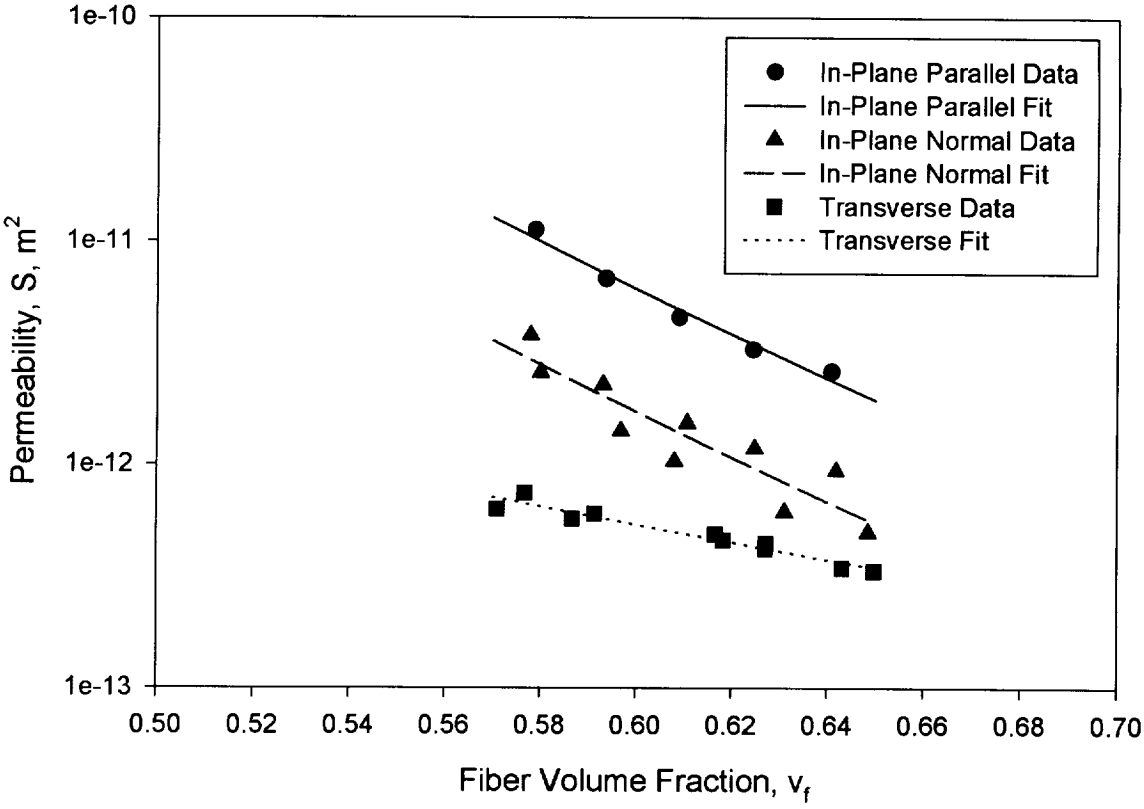

Figure 11: Permeability of Hexcel AS4/IM7 8-Stack Batch 1 Heat Set Multiaxial Warp Knit Fabric.

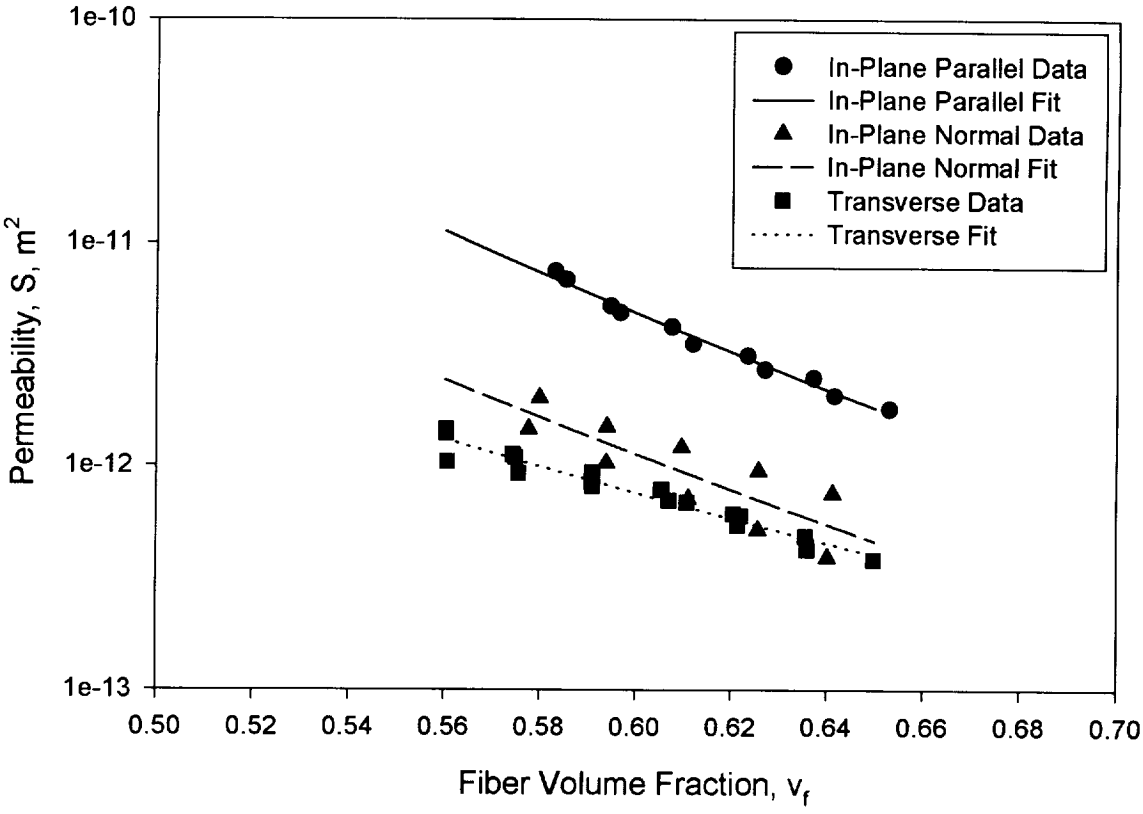

Figure 12: Permeability of Hexcel AS4/IM7 16-Stack Multiaxial Warp Knit Fabric.

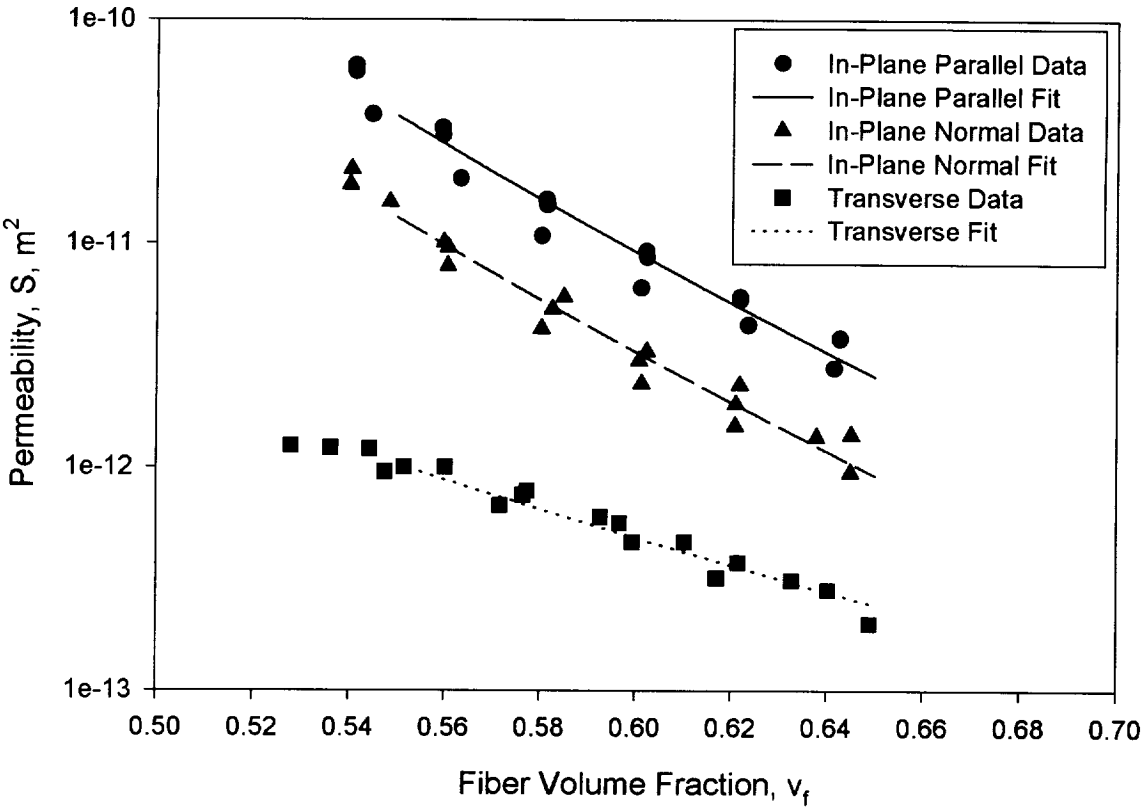

Figure 13: Permeability of 4-Tube Triaxial Braided Fabric.

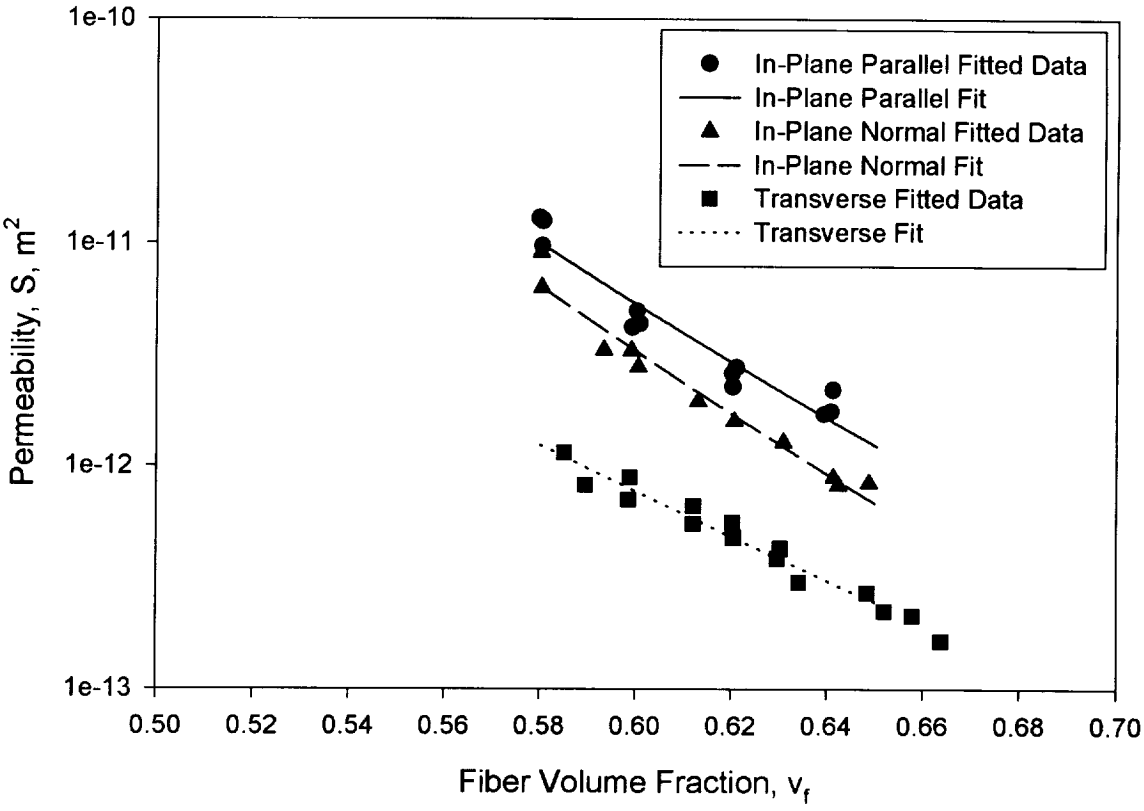

Figure 14: Permeability of 14-Tube Triaxial Braided Fabric.

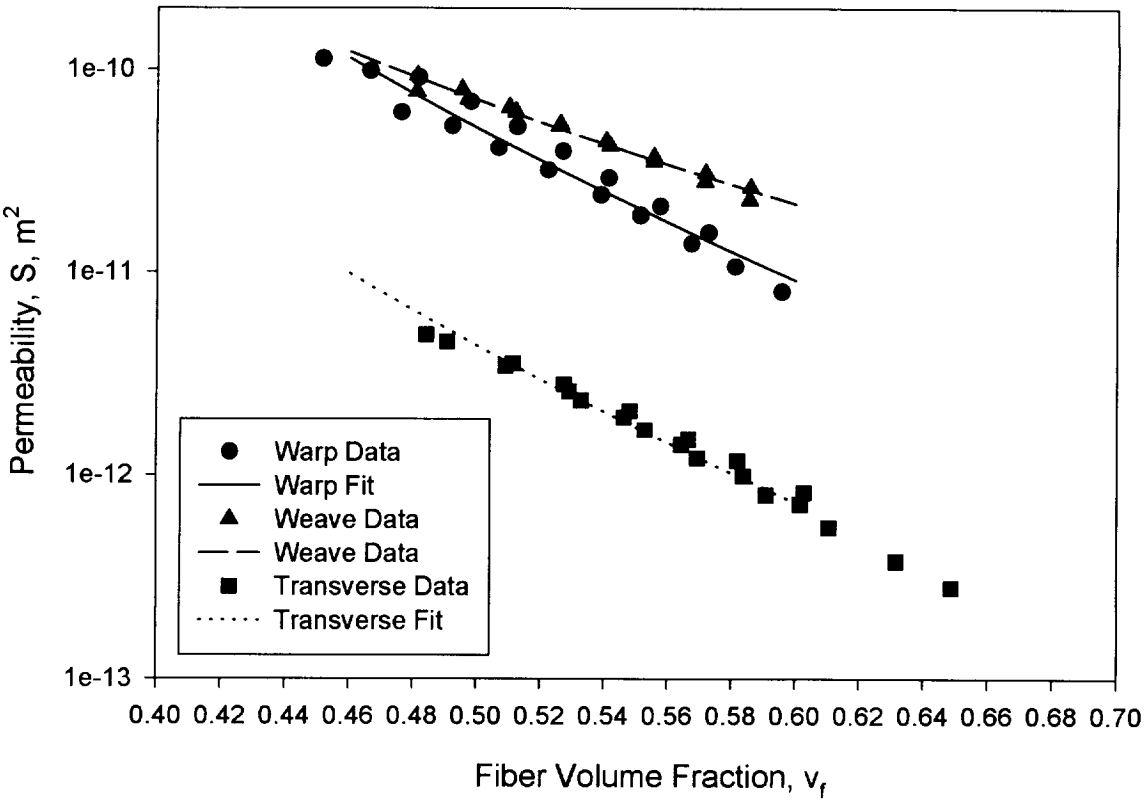

Figure 15: Permeability of Knytex 7544 Fabric (10 Ply).

Table 8: Permeability Fit Constants for Hexcel AS4/IM7 MAWK

	a	b
4-stack		
$\parallel$ to stitching	1.60×10^{-14}	-11.82
$\perp$ to stitching	4.80×10^{-15}	-11.02
TTT	3.22×10^{-14}	-5.85
8-stack batch 1		
$\parallel$ to stitching	9.94×10^{-15}	-12.45
$\perp$ to stitching	1.75×10^{-15}	-12.63
TTT	4.33×10^{-14}	-5.47
8-stack batch 2		
$\parallel$ to stitching	1.34×10^{-14}	-12.26
$\perp$ to stitching	2.87×10^{-15}	-12.41
TTT	2.83×10^{-14}	-6.40
8-stack batch 1 heat set		
$\parallel$ to stitching	4.02×10^{-15}	-14.34
$\perp$ to stitching	1.13×10^{-15}	-14.33
TTT	3.23×10^{-14}	-5.50
16-stack		
$\parallel$ to stitching	9.32×10^{-15}	-12.24
$\perp$ to stitching	3.65×10^{-15}	-11.22
TTT	1.25×10^{-14}	-8.02

2.2 Permeability Results

The 6-stack Hexcel AS4 preforms were stitched at four different stitch densities to evaluate the effect of stitch spacing on permeability characteristics. The rows of stitches were spaced either 0.2, 0.3, 0.5 or 0.75 inches apart with the stitch step remaining constant at 1/8 inch. As can be seen in Figures 16 - 18 there is no apparent trend in the permeability versus fiber volume fraction curves with stitch density. The permeability versus fiber volume fraction data for four different stitch densities are shown in Figures 19- 21. The solid line represents the power-law fit to the table. The dashed lines represent one standard deviation from the mean.

Table 9: Permeability Fit Constants for Braided Material

	a	b
14-Tube		
$\parallel$ to stitching	4.76×10^{-16}	-18.26
$\perp$ to stitching	1.36×10^{-16}	-19.76
TTT	5.40×10^{-16}	-14.21
4-Tube		
$\parallel$ to stitching	2.52×10^{-15}	-16.05
$\perp$ to stitching	9.8×10^{-16}	-15.88
TTT	5.88×10^{-15}	-8.63

Table 10: Permeability Fit Constants for Glass Fabric

	a	b
Knytex 7544 10-ply		
Warp	7.17×10^{-14}	-9.48
Fill	7.75×10^{-13}	-6.51
TTT	4.99×10^{-15}	-9.77
Boeing 7544 (from lit.)	4.8907×10^{-15}	-7.2111

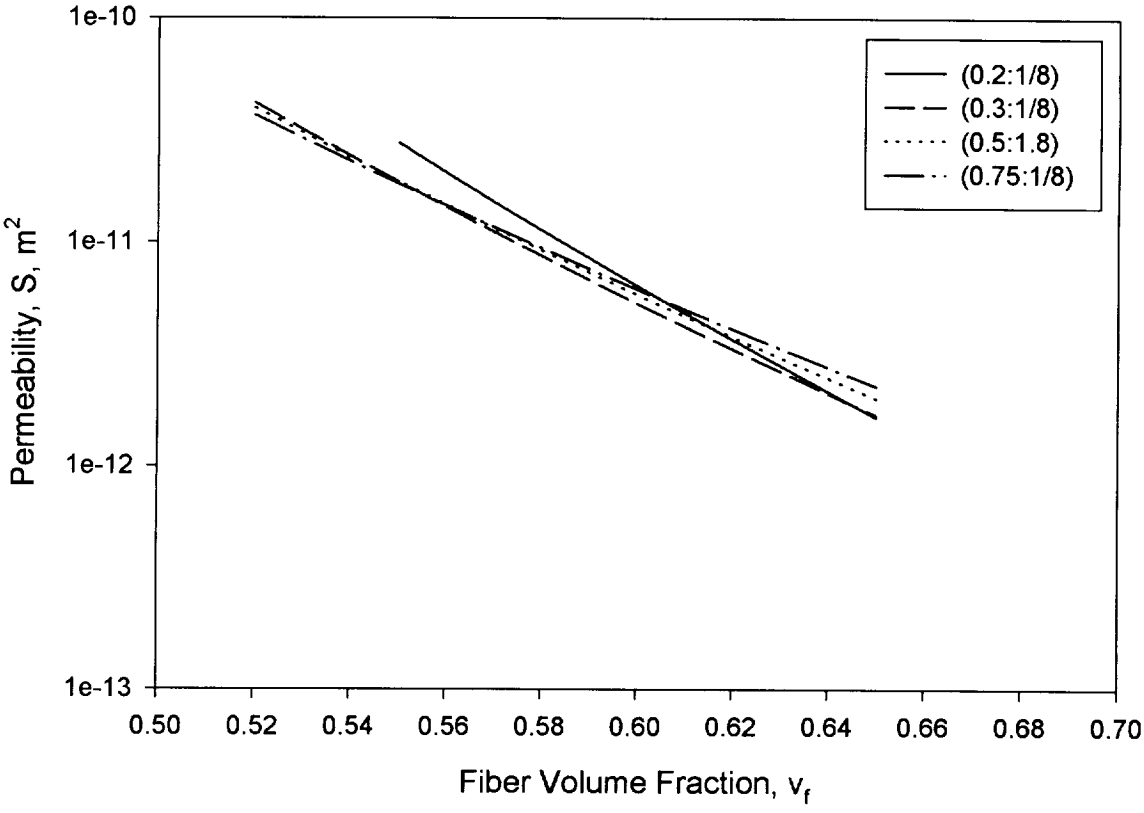

Figure 16: Effect of Stitch Density on In-Plane Permeability Parallel to the Stitching in 6-stack Hexcel AS4 Preforms - Individual Fits.

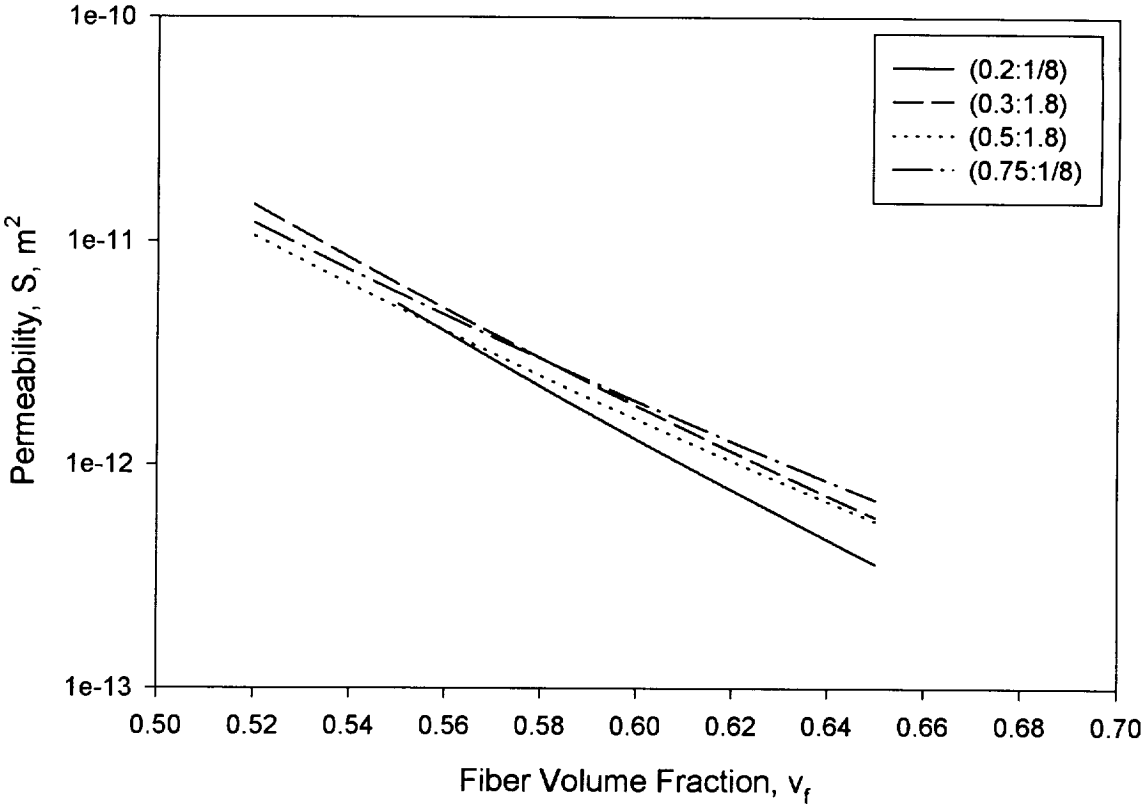

Figure 17: Effect of Stitch Density on In-Plane Permeability Normal to the Stitching in 6-stack Hexcel AS4 Preforms - Individual Fits.

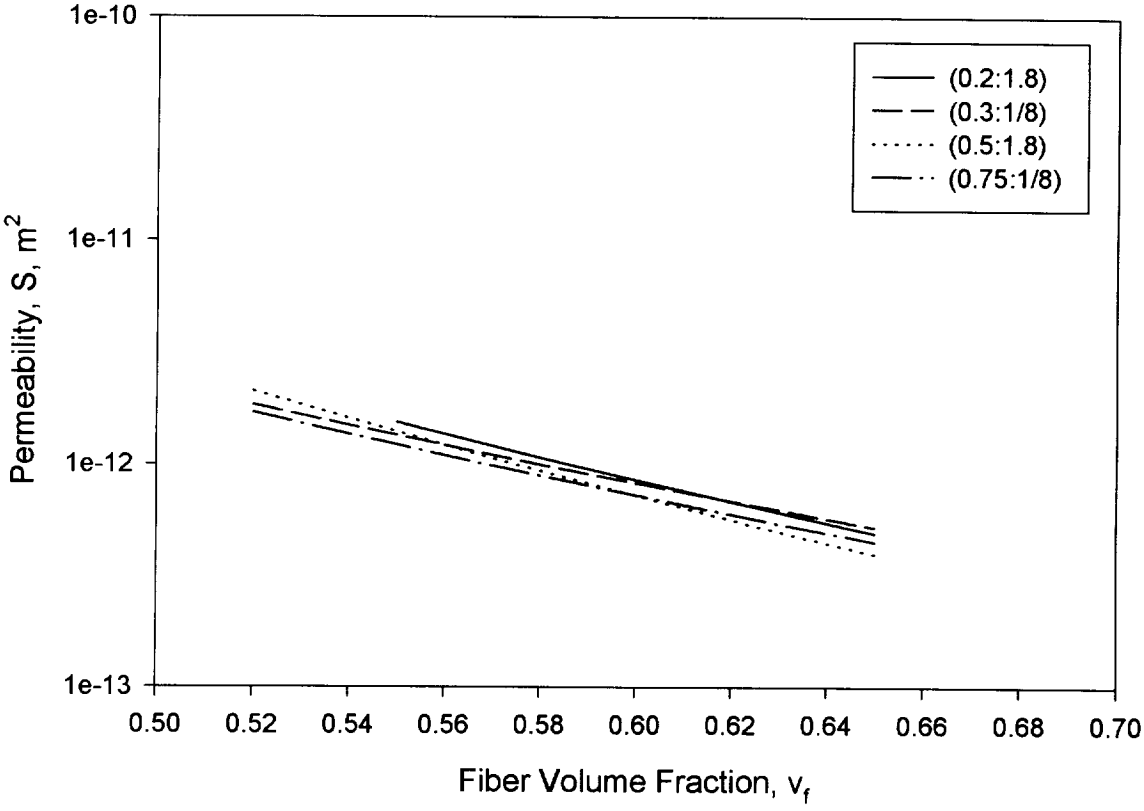

Figure 18: Effect of Stitch Density on Transverse Permeability in 6-stack Hexcel AS4 Preforms - Individual Fits.

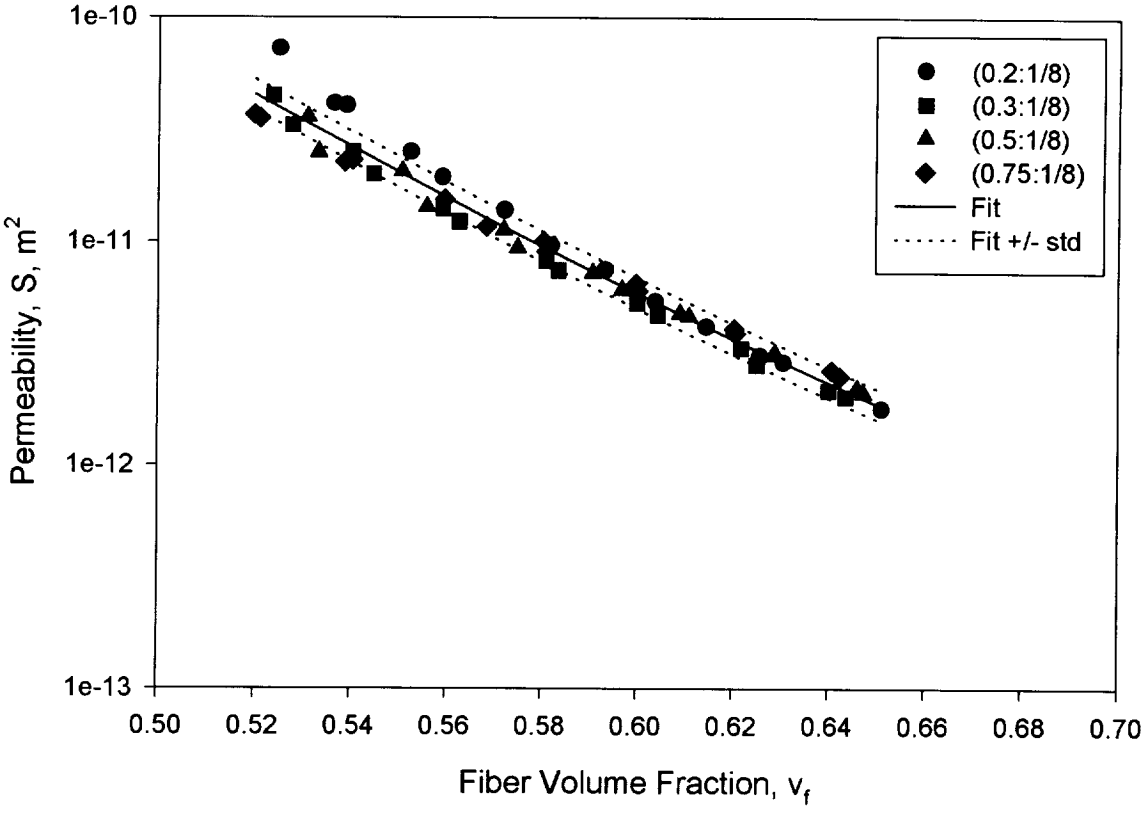

Figure 19: Effect of Stitch Density on In-Plane Permeability Parallel to the stitching in 6-stack Hexcel AS4 Preforms.

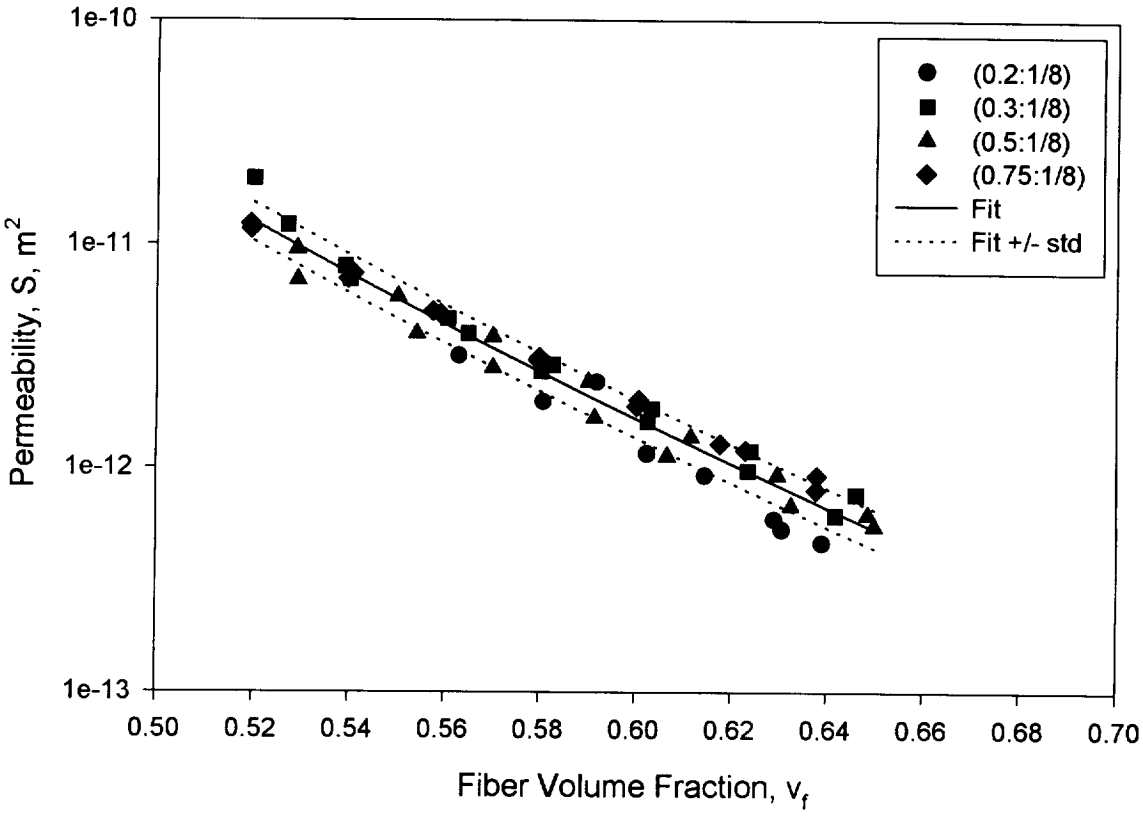

Figure 20: Effect of Stitch Density on In-Plane Permeability Normal to the Stitching in 6-stack Hexcel AS4 Preforms.

The effect of preform thickness on permeability behavior was investigated in the AS4/IM7 MAWK fabric and the Triaxial Braid Fabric. Hexcel AS4/IM7 Multiaxial Warp Knit Fabric preforms with thicknesses of 4-stack, 8-stack, and 16-stack were tested. The power-law fits to the in-plane permeability data parallel to the stitching tend to indicate that as the preform thickness increases the magnitude of the permeability decreases. The rate of decrease with increasing fiber volume fraction appears to be approximately constant. This can be seen in Figure 22. This trend, however, is not evident in the in-plane permeability normal to the stitching or in the permeability transverse to the stitching as seen in Figures 23 and 24. Figures 25- 27 show the power-law curve fit to all the fiber volume fraction vs. permeability data regardless of preform thickness, in each of the three directions.

The triaxial braid was tested in two thicknesses, 4-tube and 14-tube. There is a visible difference in the power-law fit to the permeability data for the two thicknesses parallel to

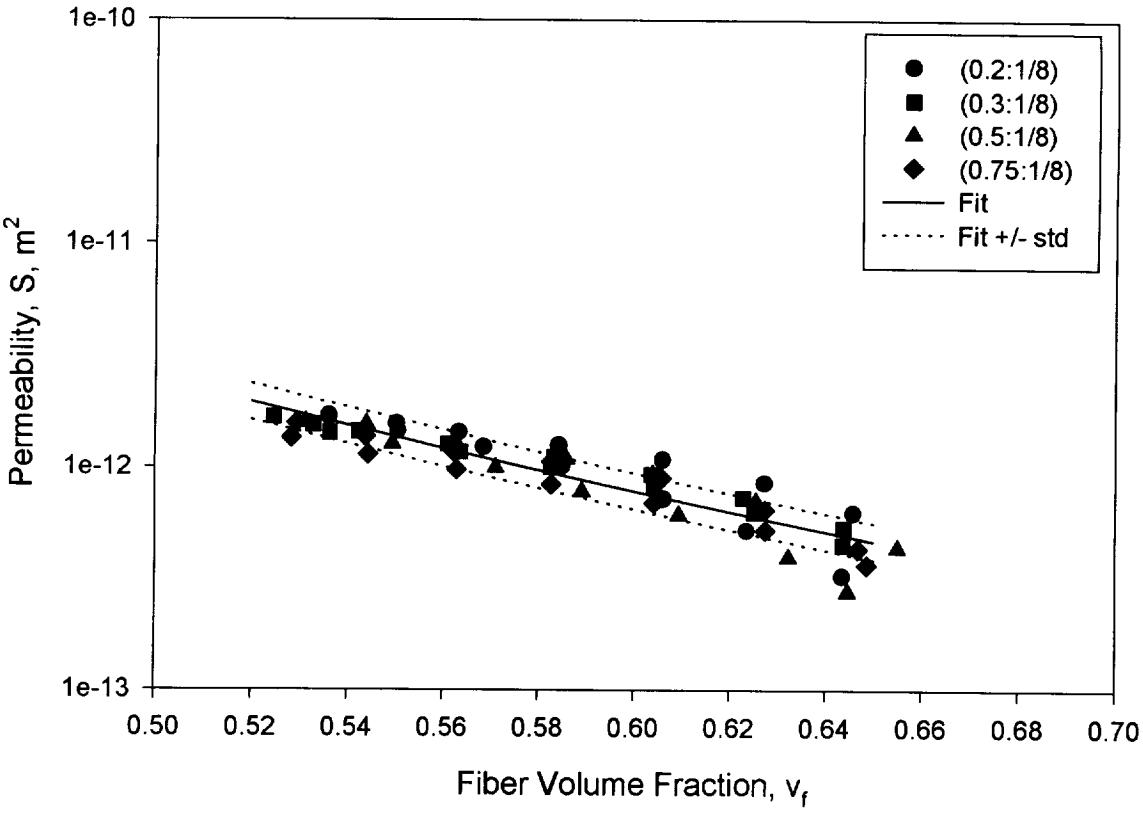

Figure 21: Effect of Stitch Density on Transverse Permeability in 6-stack Hexcel AS4 Preforms.

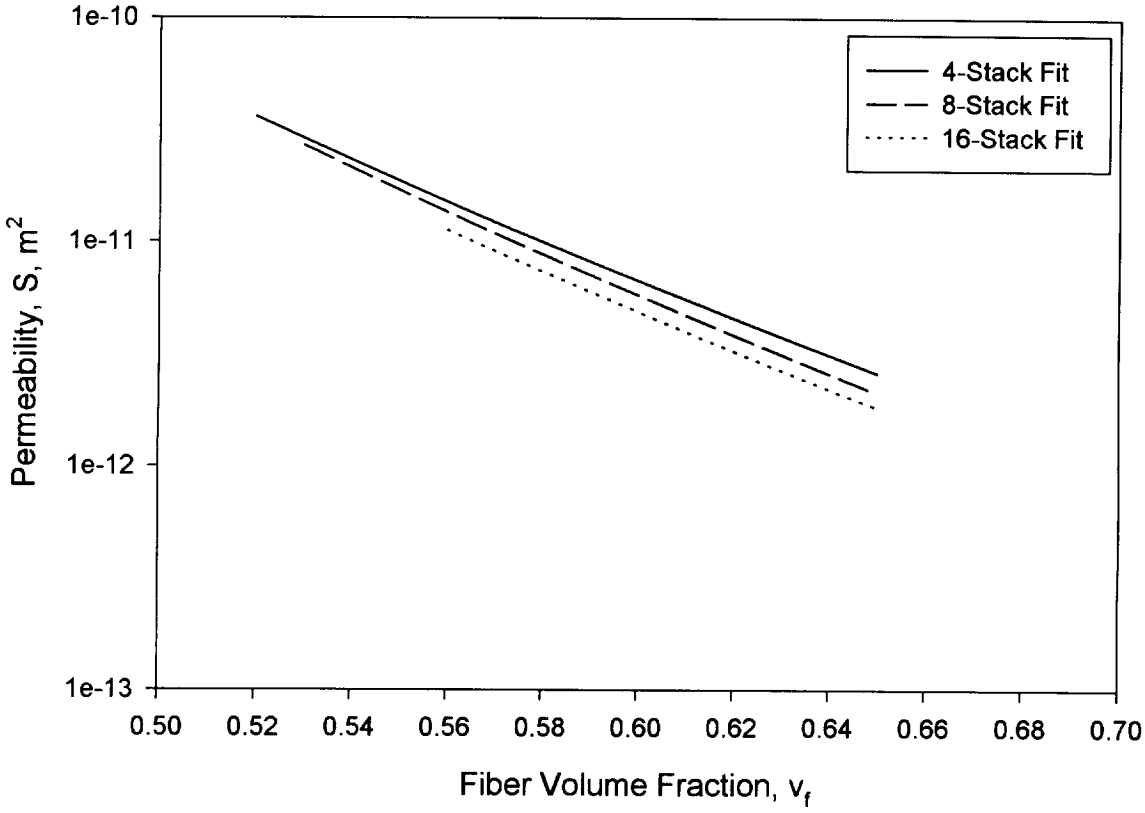

Figure 22: Effect of Thickness on In-Plane Permeability Parallel to the stitching in Hexcel AS4/IM7 Preforms - Individual Fits.

the stitching and transverse to the stitching as seen in Figures 28 and 30. In the in-plane normal to the stitching direction, however, there is not a clear effect of thickness as seen in Figure 29. Figures 31- 33 show the data from both thicknesses and the power-law fit to all the data in each of the three directions.

The effect of batch variability on permeability behavior was investigated by testing preforms from two batches of the 8-stack AS4/IM7 Multiaxial Warp Knit material. It is seen in Figures 34- 36 that there are variations in the measured permeabilities from two different batches of the same material. However, often the variation in measured permeability between two samples from the same batch is equal to or greater than the variation between two samples from different batches as is seen in Figure 35.

Parts fabricated by RFI are often heat set before being infiltrated with resin. In the heat set procedure, the part is laid up without the resin and subjected to an abbreviated

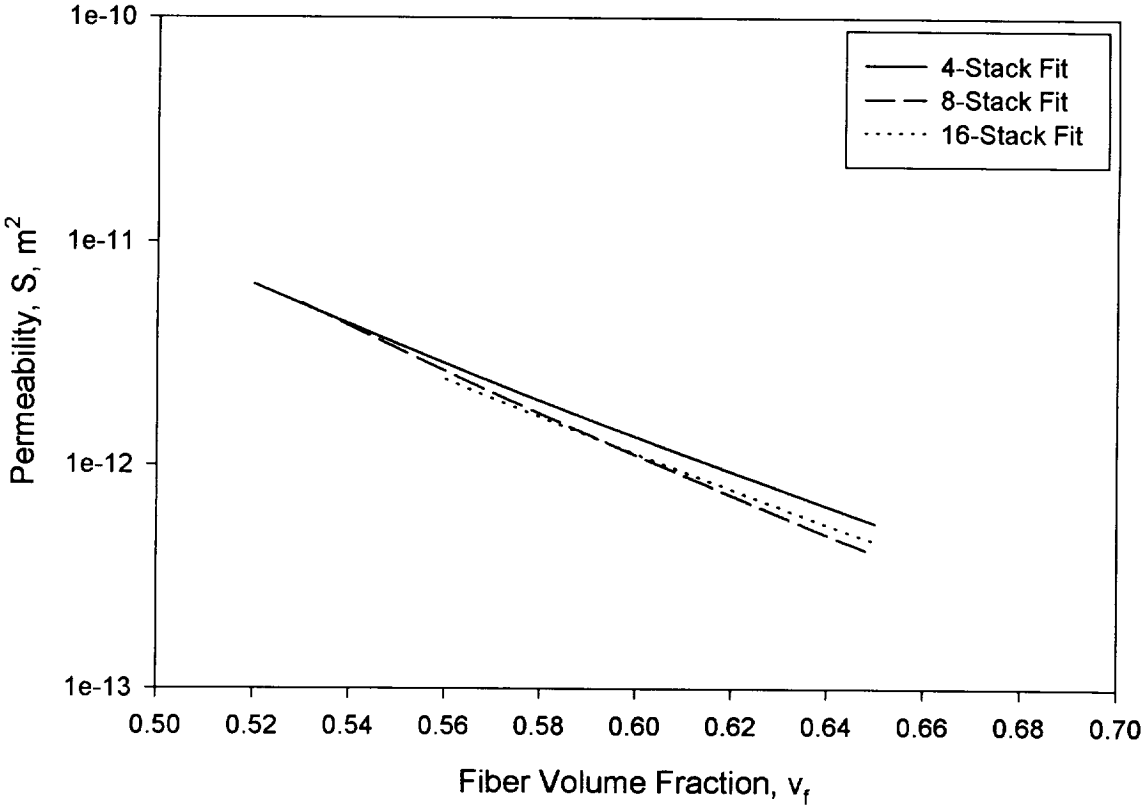

Figure 23: Effect of Thickness on In-Plane Permeability Normal to the Stitching in Hexcel AS4/IM7 Preforms - Individual Fits.

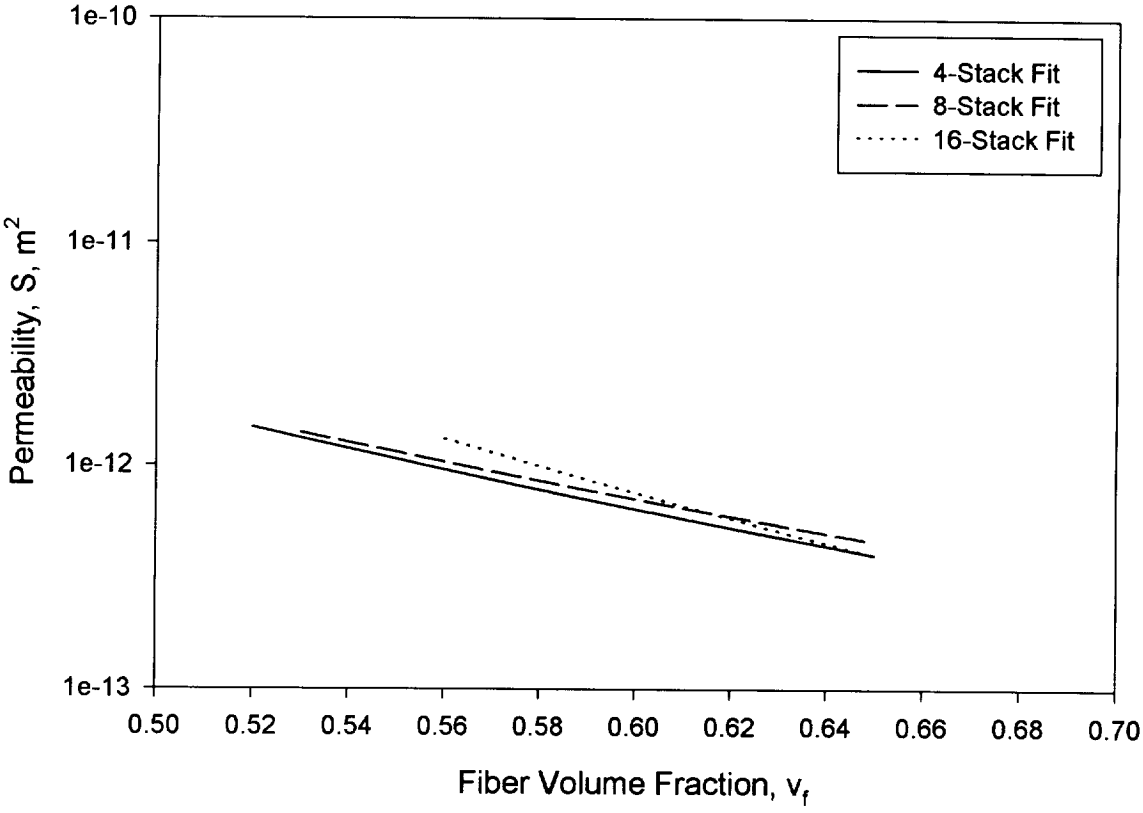

Figure 24: Effect of Thickness on Transverse Permeability in Hexcel AS4/IM7 Preforms - Individual Fits.

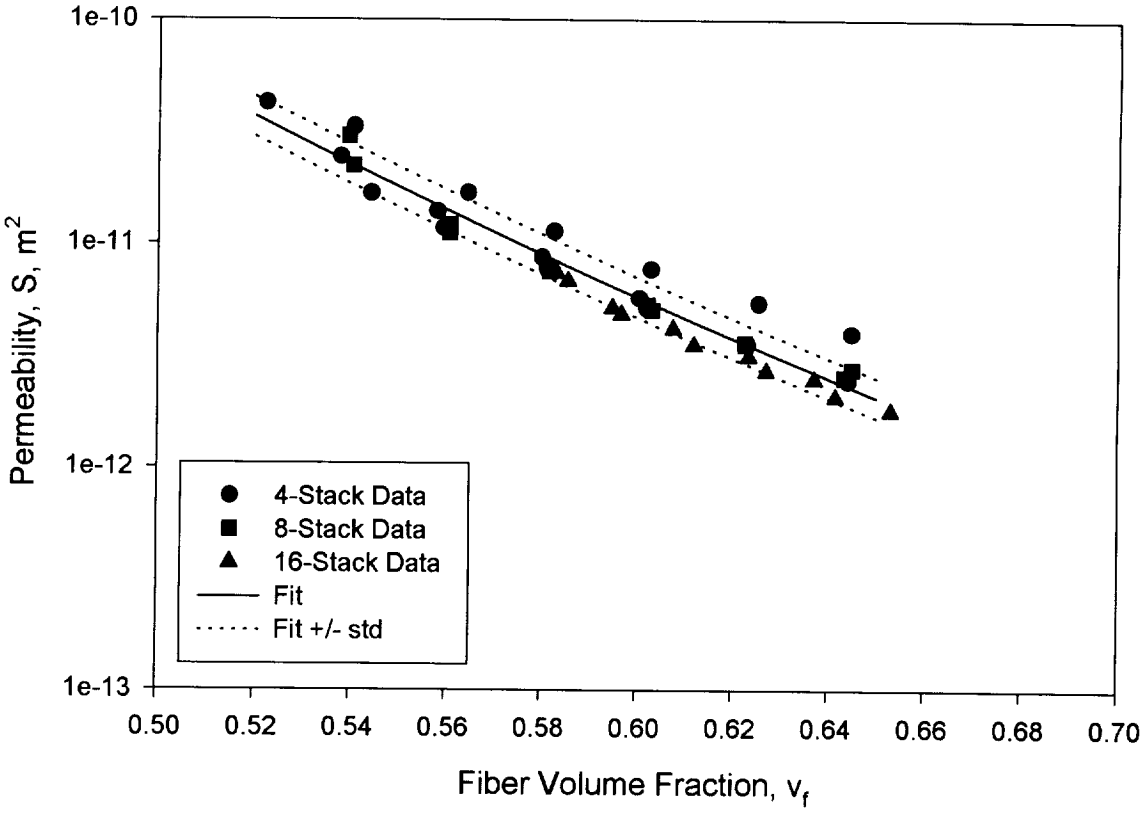

Figure 25: Effect of Thickness on In-Plane Permeability Parallel to the Stitching in Hexcel AS4/IM7 Preforms.

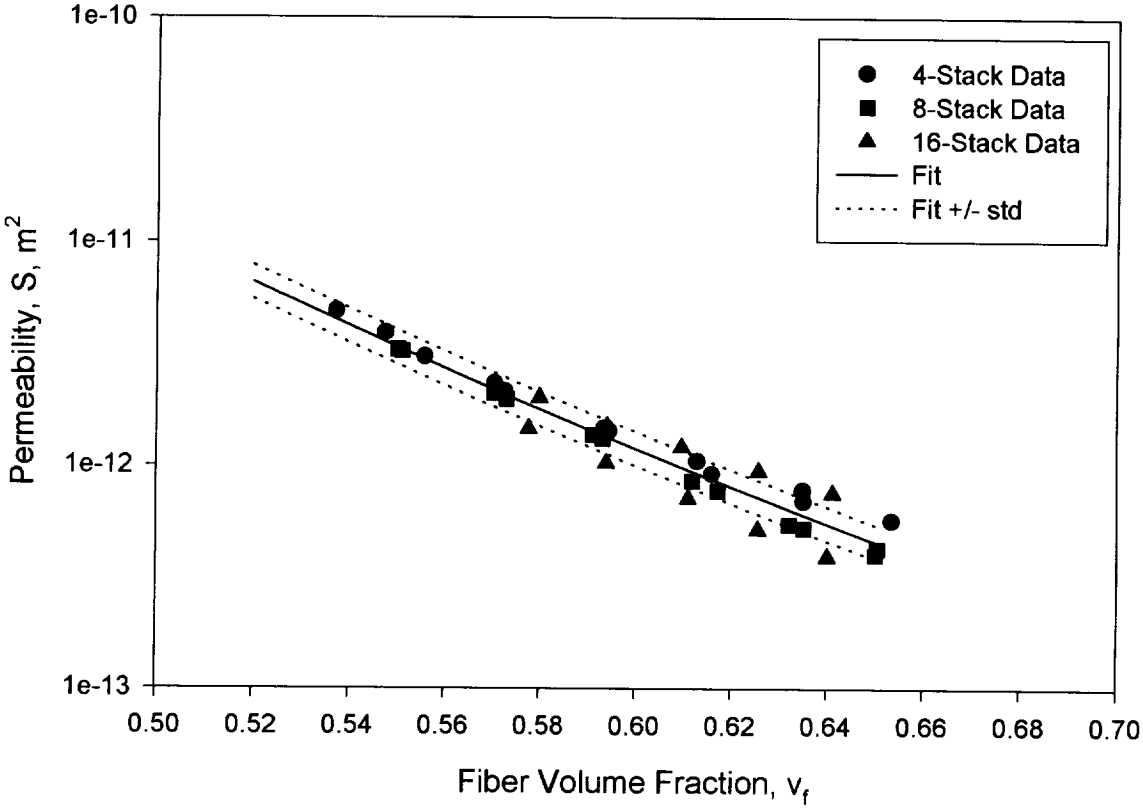

Figure 26: Effect of Thickness on In-Plane Permeability Normal to the Stitching in Hexcel AS4/IM7 Preforms.

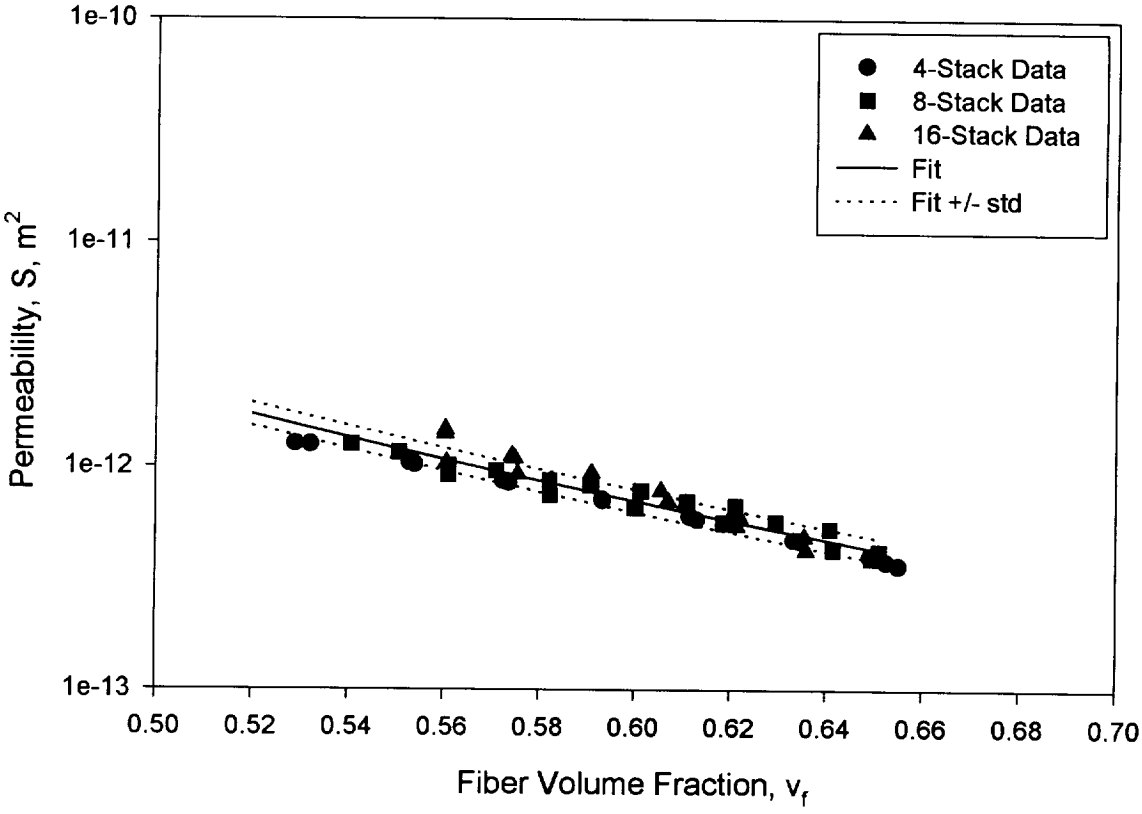

Figure 27: Effect of Thickness on Transverse Permeability in Hexcel AS4/IM7 Preforms.

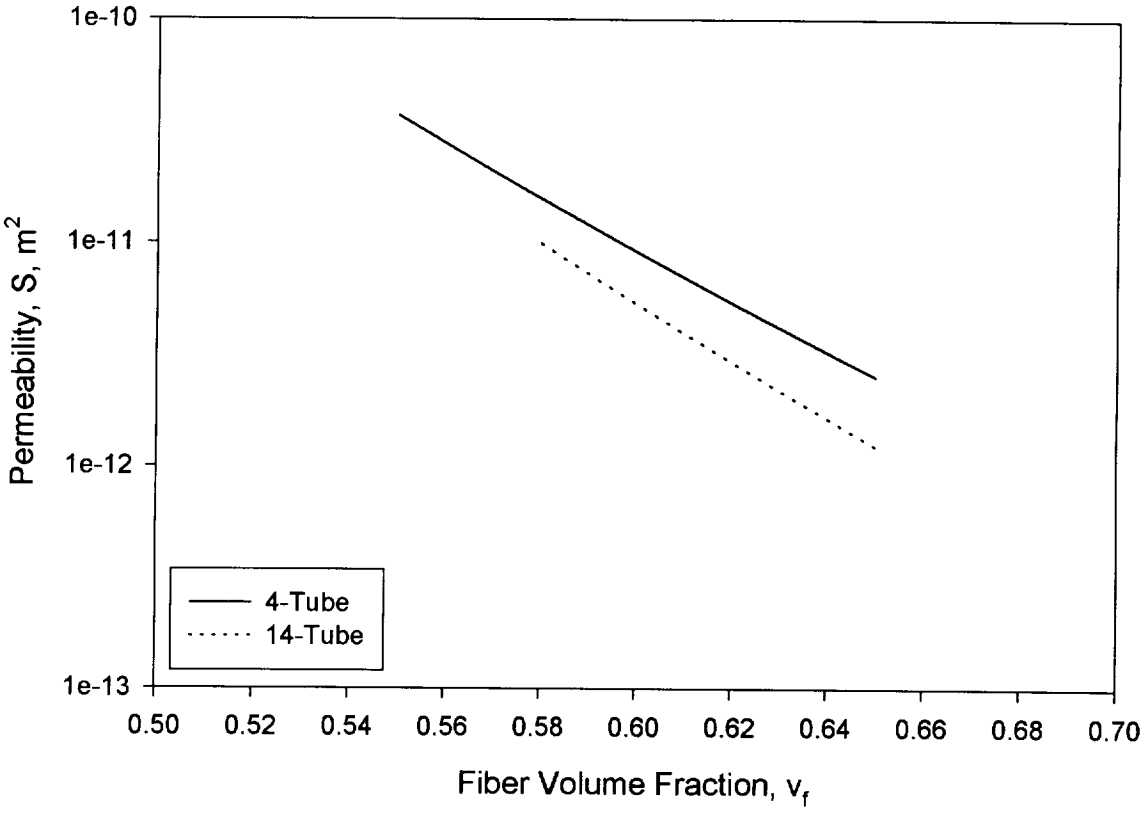

Figure 28: Effect of Thickness on In-Plane Permeability Parallel to the Stitching in Triaxial Braid Preforms - Individual Fits.

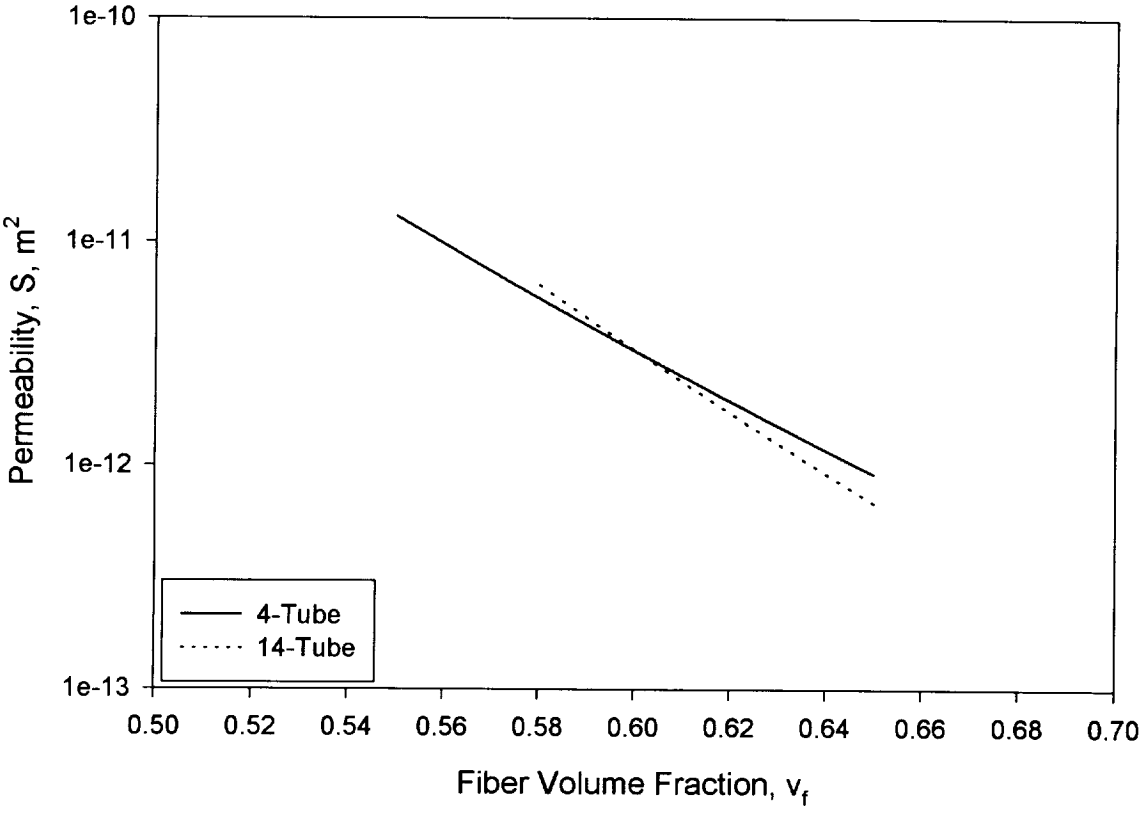

Figure 29: Effect of Thickness on In-Plane Permeability Normal to the Stitching in Triaxial Braid Preforms - Individual Fits.

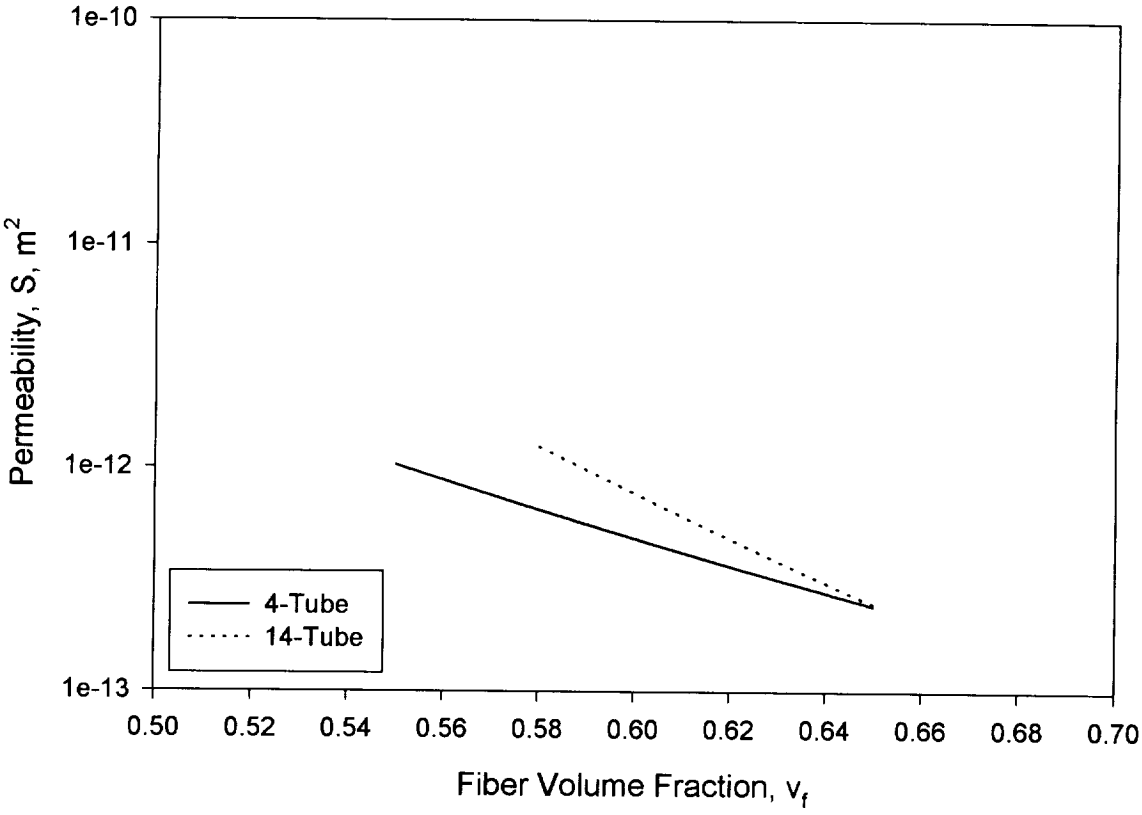

Figure 30: Effect of Thickness on Transverse Permeability in Triaxial Braid Preforms - Individual Fits.

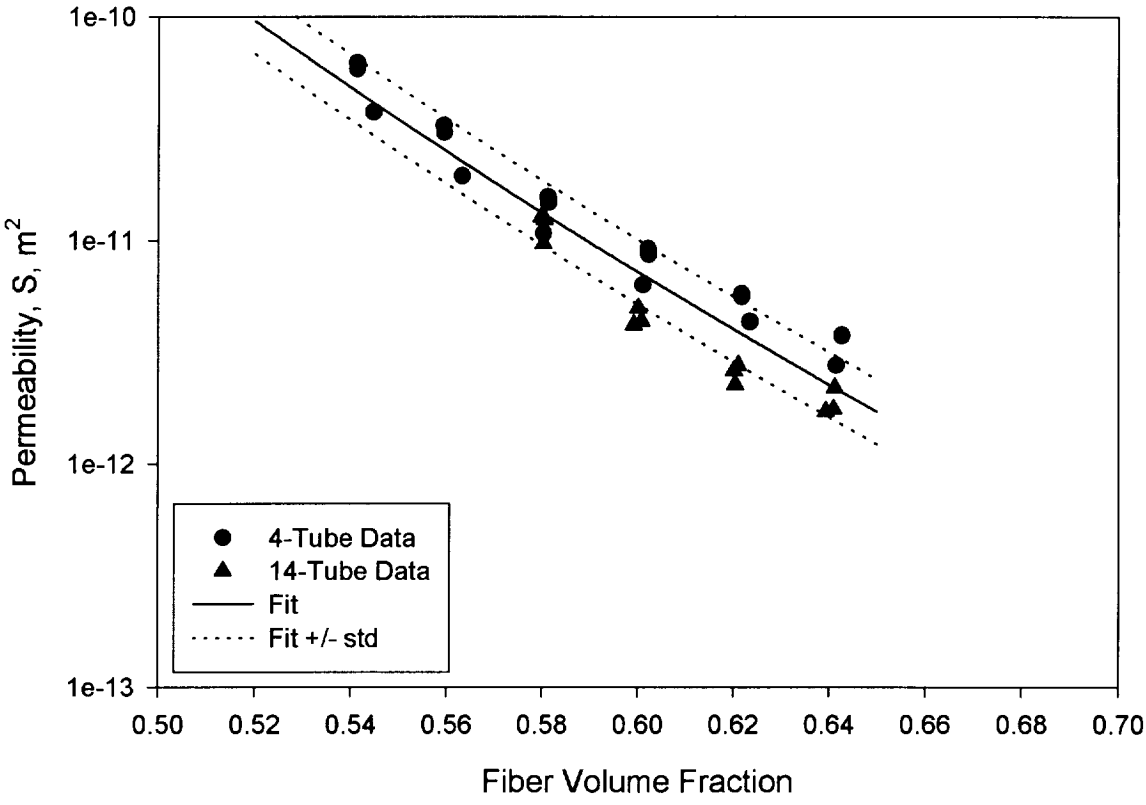

Figure 31: Effect of Thickness on In-Plane Permeability Parallel to the stitching in Triaxial Braid Preforms.

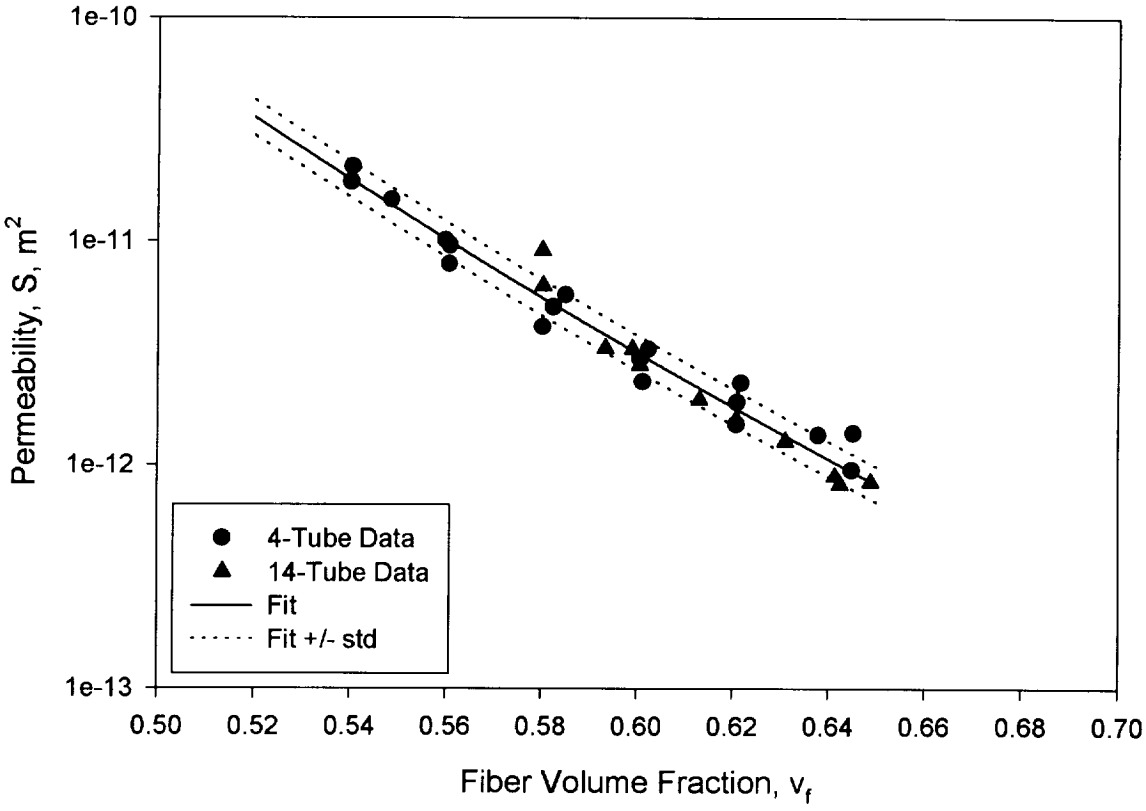

Figure 32: Effect of Thickness on In-Plane Permeability Normal to the Stitching in Triaxial Braid Preforms.

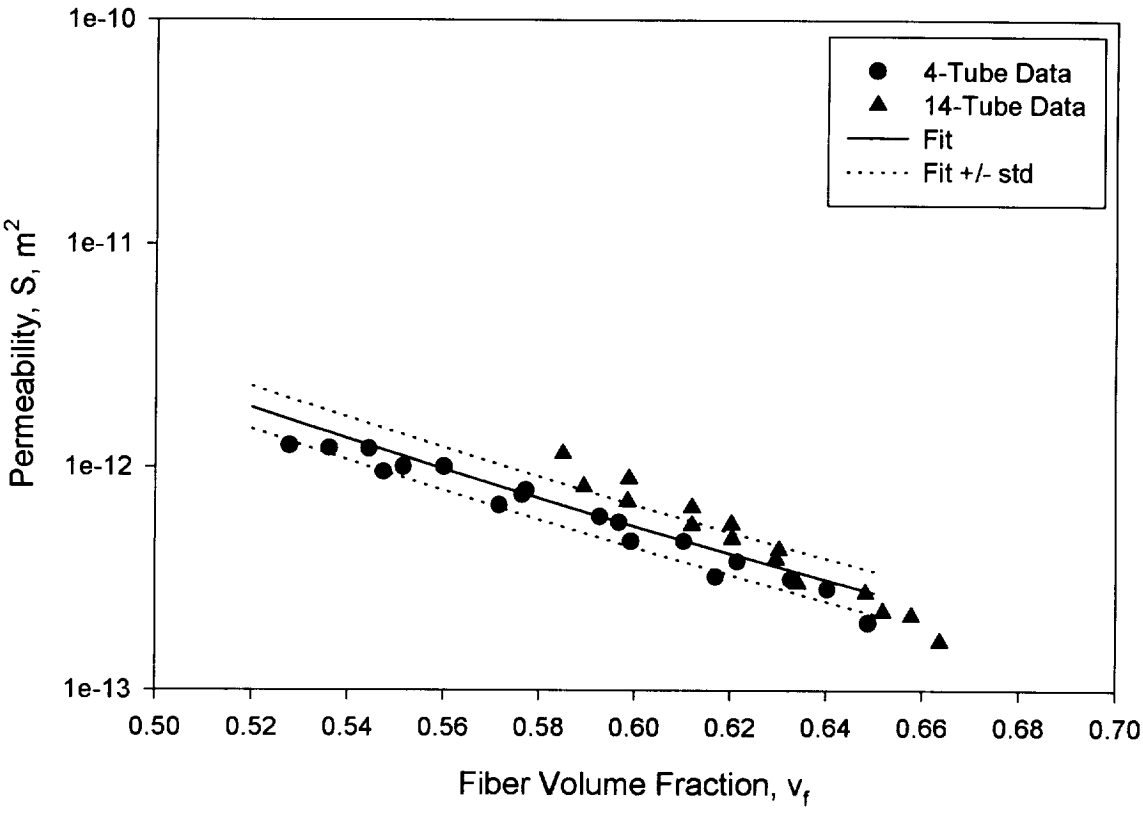

Figure 33: Effect of Thickness on Transverse Permeability in Triaxial Braid Preforms.

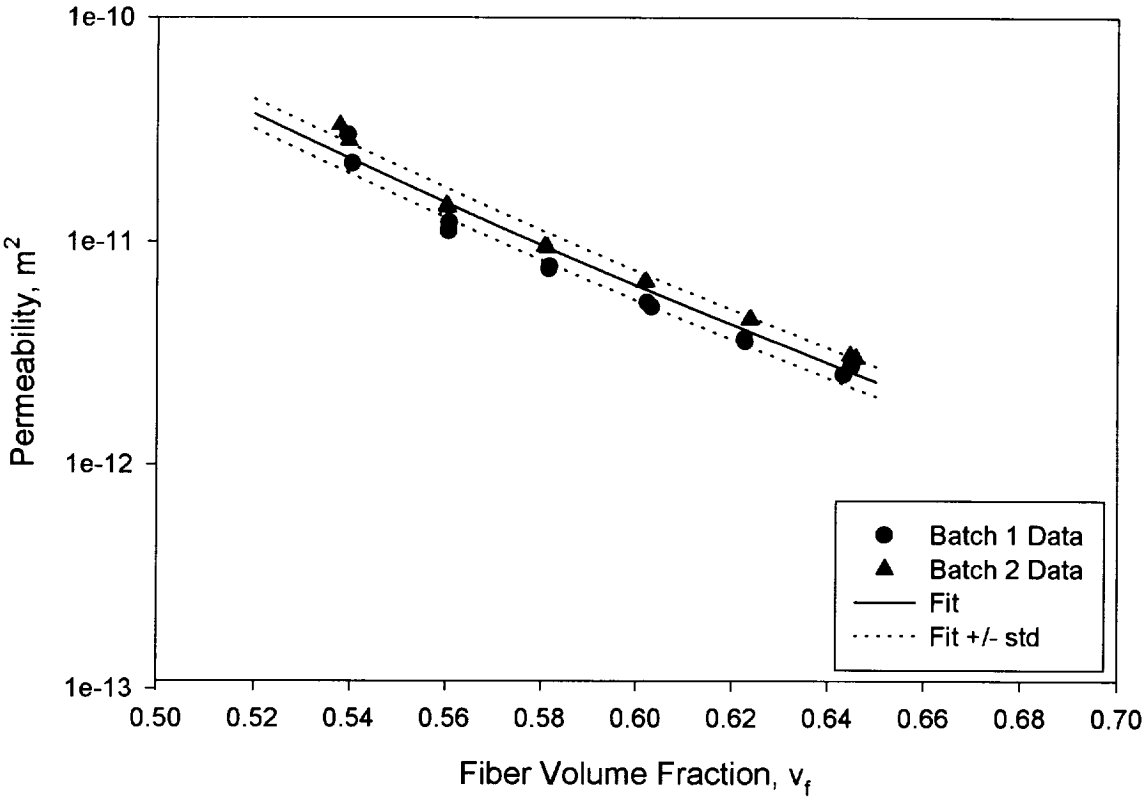

Figure 34: Effect of Batch Variability on In-Plane Permeability Parallel to the stitching in 8-stack Hexcel AS4/IM7 Preforms.

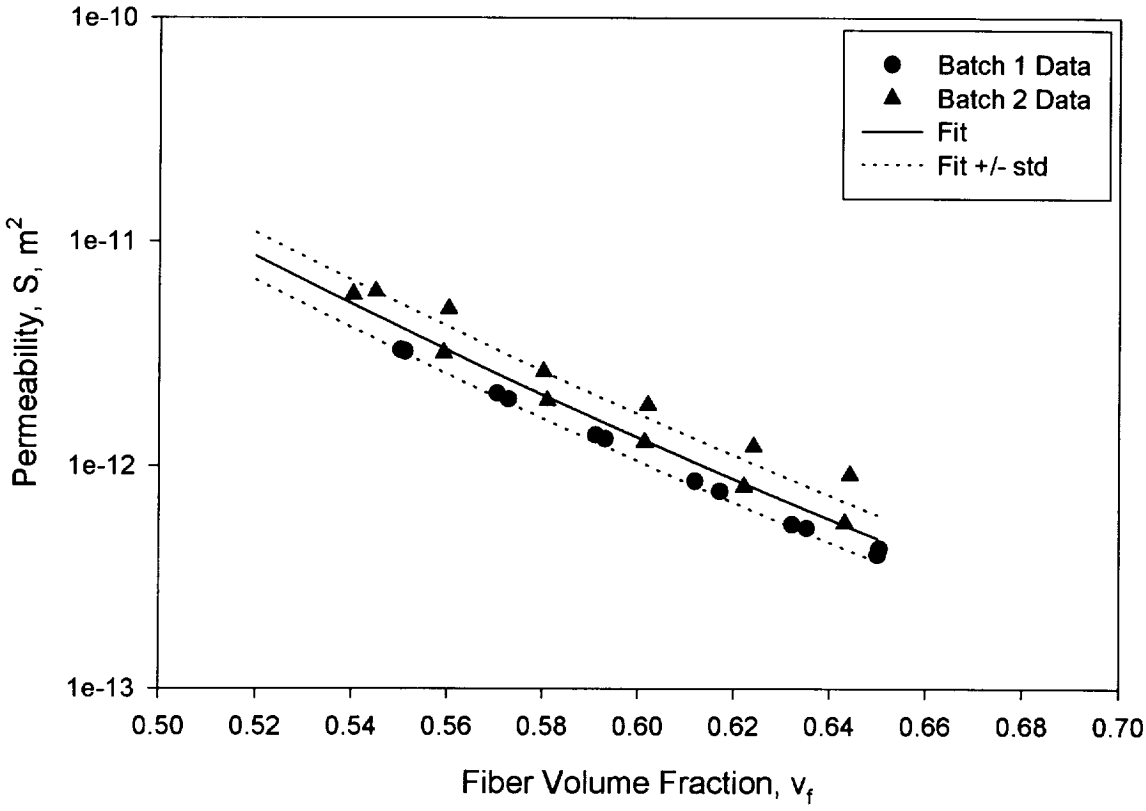

Figure 35: Effect of Batch Variability on In-Plane Permeability Normal to the Stitching in 8-stack Hexcel AS4/IM7 Preforms.

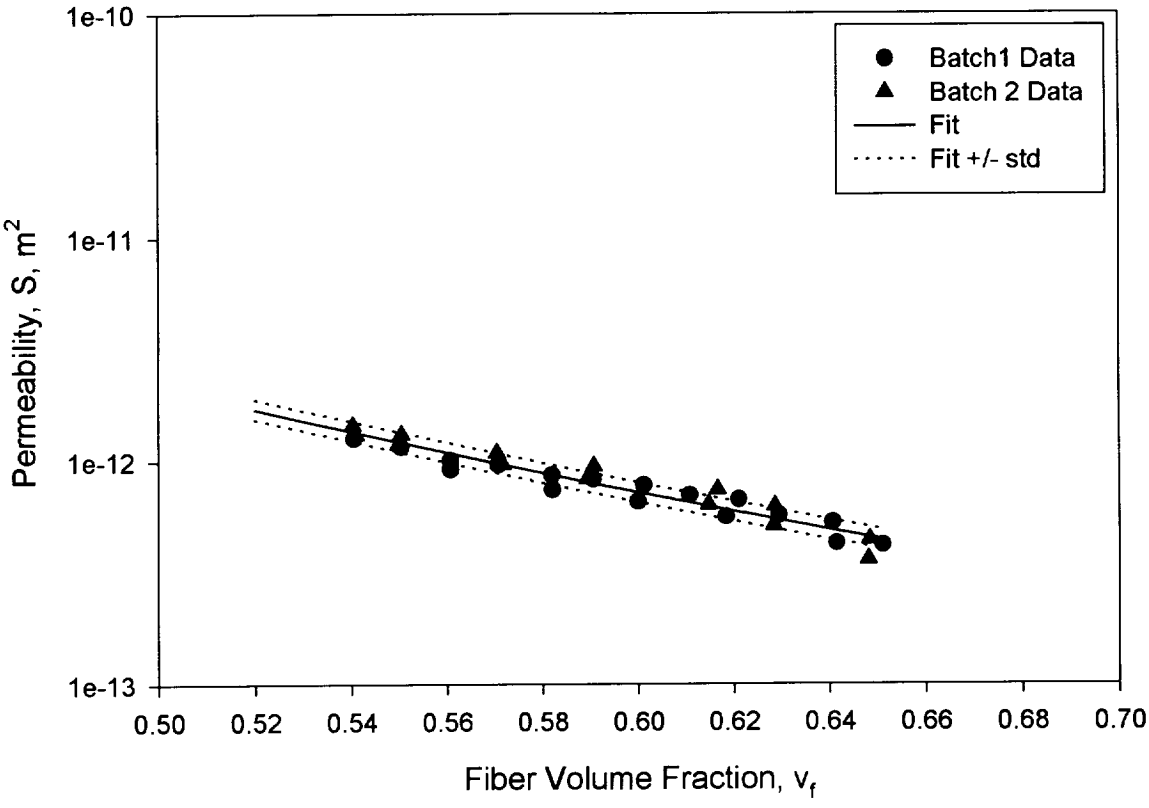

Figure 36: Effect of Batch Variability on Transverse Permeability in Hexcel 8-stack AS4/IM7 Preforms.

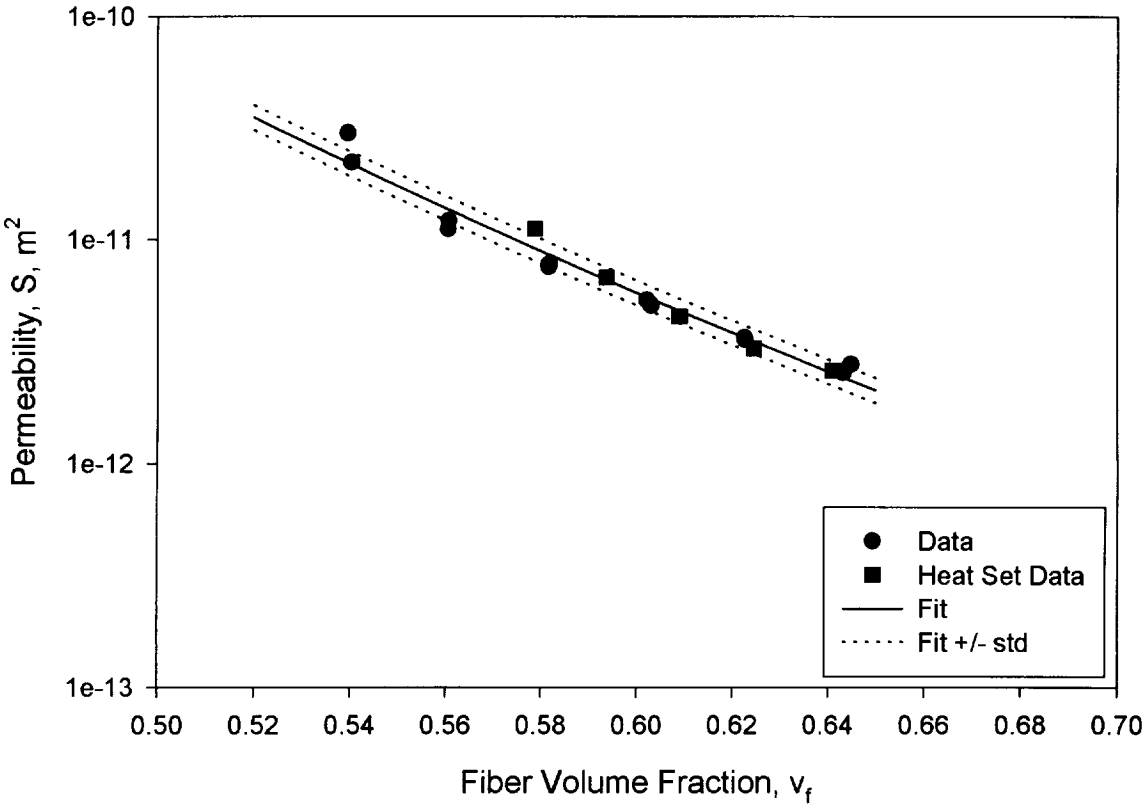

Figure 37: Effect of Heat Set on In-Plane Permeability Parallel to the Stitching in 8-stack Hexcel AS4/IM7 Preforms.

temperature and pressure cycle. Several samples of the 8-stack AS4/IM7 MAWK were heat set prior to making permeability measurements to determine the effect of the heat set process on the permeability behavior of the material. As seen in Figures 37- 39, the heat set process does not significantly influence the permeability behavior of the preform, except that the initial fiber volume fractions at which permeability measurements could be made were higher.

3 Compaction

Compaction of the preform squeezes the fibers closer together, and thus increases the fiber volume fraction in the preform. Since the permeability of the preform depends on the fiber volume fraction, it is necessary to predict the change in the fiber volume fraction as the body is compacted. Experiments were performed to obtain a relation between the fiber volume

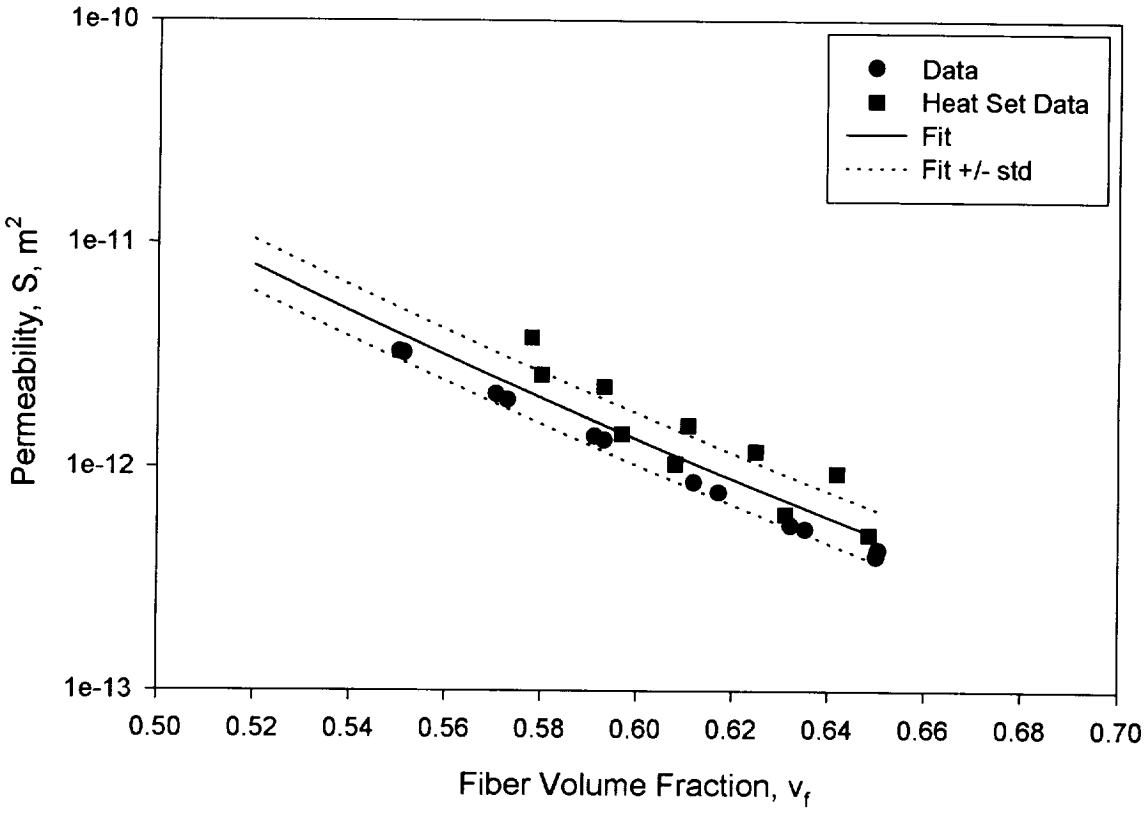

Figure 38: Effect of Heat Set on In-Plane Permeability Normal to the Stitching in 8-stack Hexcel AS4/IM7 Preforms.

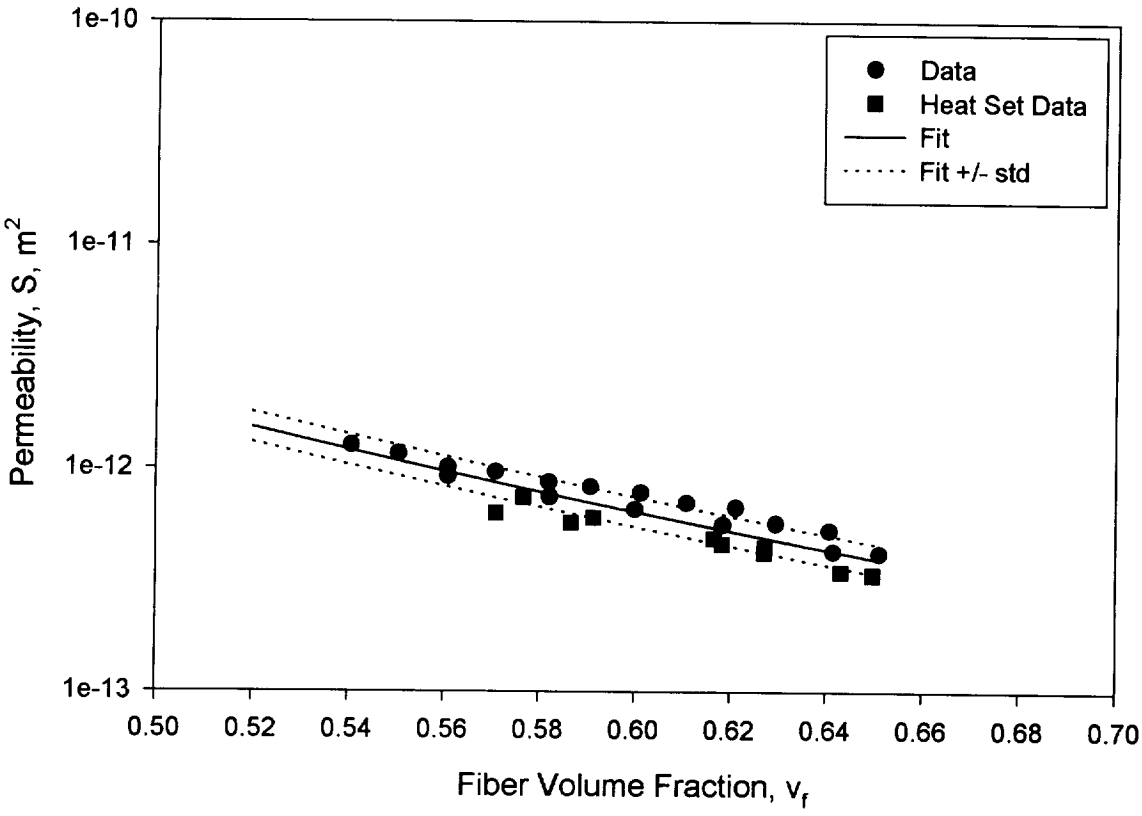

Figure 39: Effect of Heat Set on Transverse Permeability in Hexcel 8-stack AS4/IM7 Preforms.

Table 11: Test Matrix for Compaction Tests

	No. of Tests	Avg Areal Wt g/m^2	% Variation Areal Wt
Tenax HTA 8-Stack MAWK	3	1542	0.10
Hexcel AS4 (0.2:1/8) 6-Stack MAWK	2	1543	0.30
Hexcel AS4 (0.3:1/8) 6-Stack MAWK	2	1526	0.20
Hexcel AS4 (0.5:1/8) 6-Stack MAWK	2	1516	0.50
Hexcel AS4 (0.75:1/8) 6-Stack MAWK	2	1511	0.00
Hexcel AS4/IM7 4-Stack MAWK	3	1542	0.24
Hexcel AS4/IM7 8-Stack Batch 1 MAWK	2	1517	0.89
Hexcel AS4/IM7 8-Stack Batch 2 MAWK	2	1522	0.13
Hexcel AS4/IM7 8-Stack Heat Set MAWK	2	1518	0.26
Hexcel AS4/IM7 16-Stack MAWK	2	1509	0.00
4-Tube Triaxial Braid	3	1258	0.80
14-Tube Triaxial Braid	2	1287	0.20
Knytex 7544 Plain Weave Glass	2	622/ply	0.48

fraction and the state of stress in the preform. Table 11 is a summary of the number of samples of each material tested, the average areal weight of the samples, and the percent variation of the areal weight from the average.

3.1 Compaction Measurements

The in-plane permeability fixture, with the O-ring removed, was used to measure the compaction behavior. Tests were conducted using a dry preform. To determine the compaction behavior, compaction pressure is applied at a 0.508 mm/min cross head rate until the minimum desired fiber volume fraction is reached. At that point, loading is stopped and the fibers are allowed to relax, and realign themselves. When the relaxation has ceased as indicated by the load becoming steady, the compaction pressure and fiber volume fraction are recorded. The load is then increased until the next desired fiber volume fraction is reached. For the tests conducted, data were taken at fiber volume fractions in the range of 50–64%. The data acquisition system used for the permeability test was also used in the compaction experiments. The data were fit with the fourth order polynomial

$$v_f = a_0 + a_1\bar{\sigma} + a_2\bar{\sigma}^2 + a_3\bar{\sigma}^3 + a_4\bar{\sigma}^4 \tag{3}$$

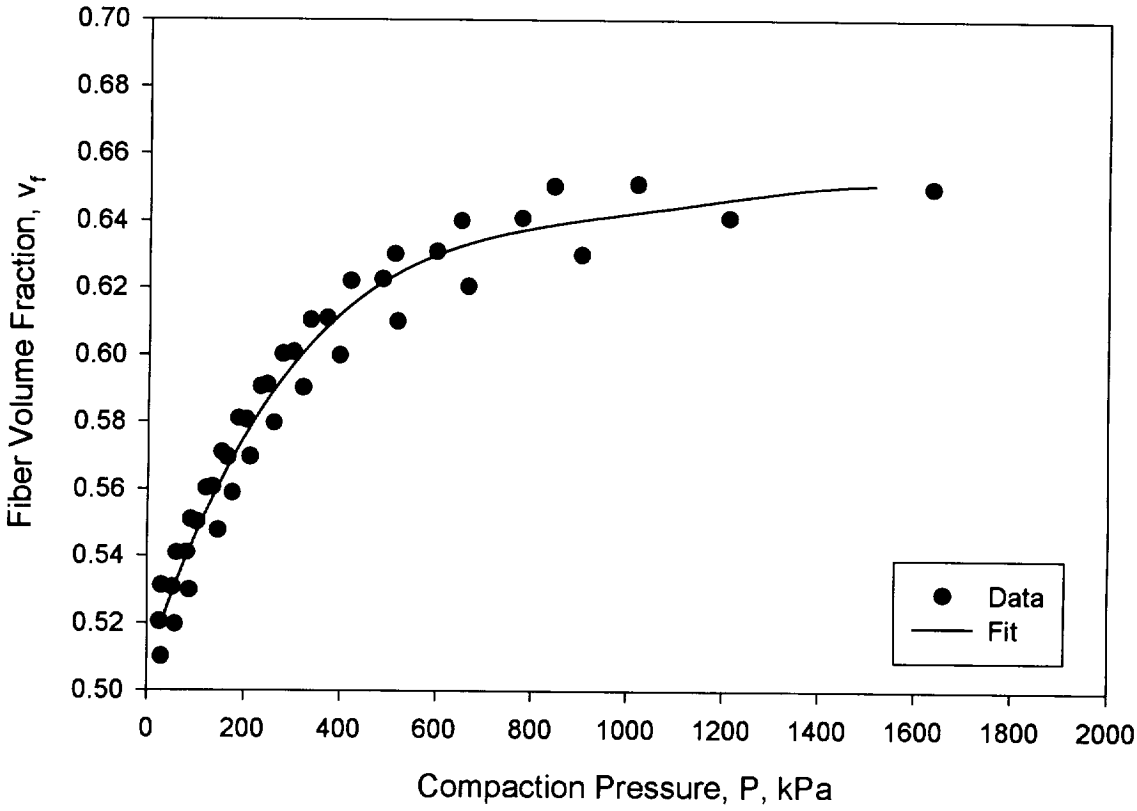

Figure 40: Compaction Behavior of Tenax HTA Multiaxial Warp Knit Fabric.

where a_i are constants, and $\bar{\sigma}$ is the effective stress, or the stress in the thickness direction of the material in units of kPa. Figures 40 - 51 show the data and fourth order polynomial fits for the materials tested.

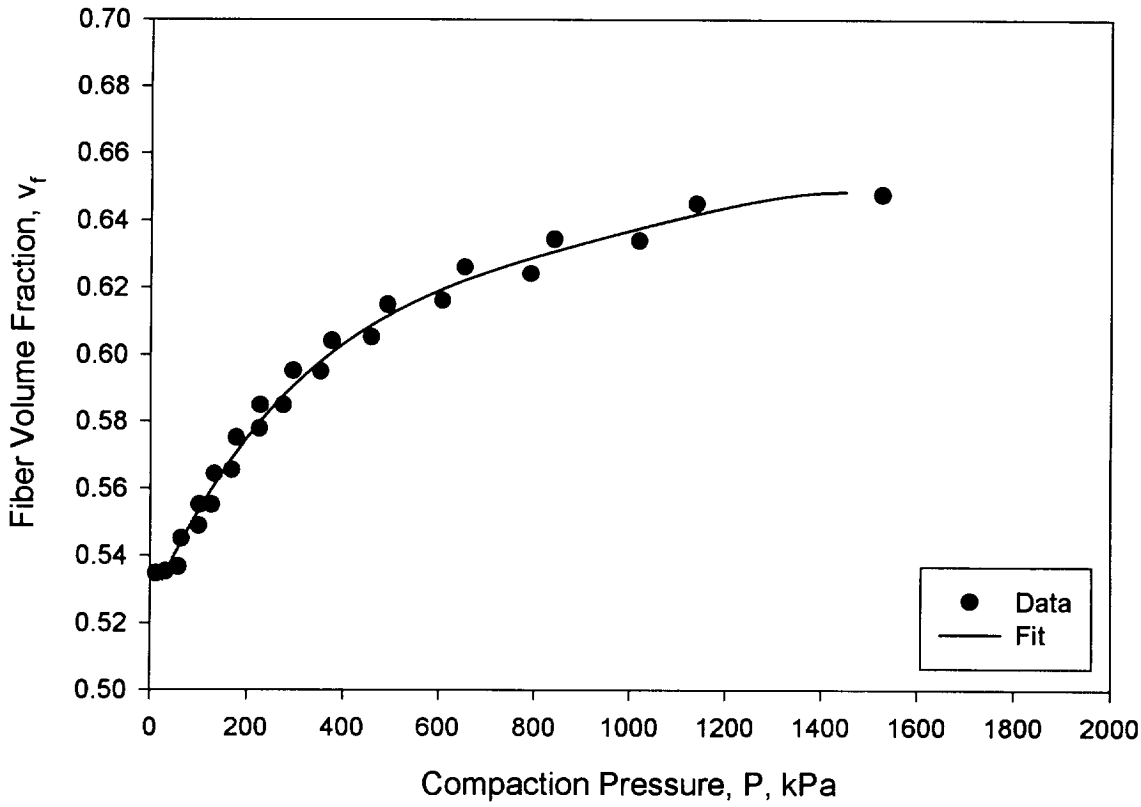

Figure 41: Compaction Behavior of Hexcel AS4 (0.2:1/8) Multiaxial Warp Knit Fabric.

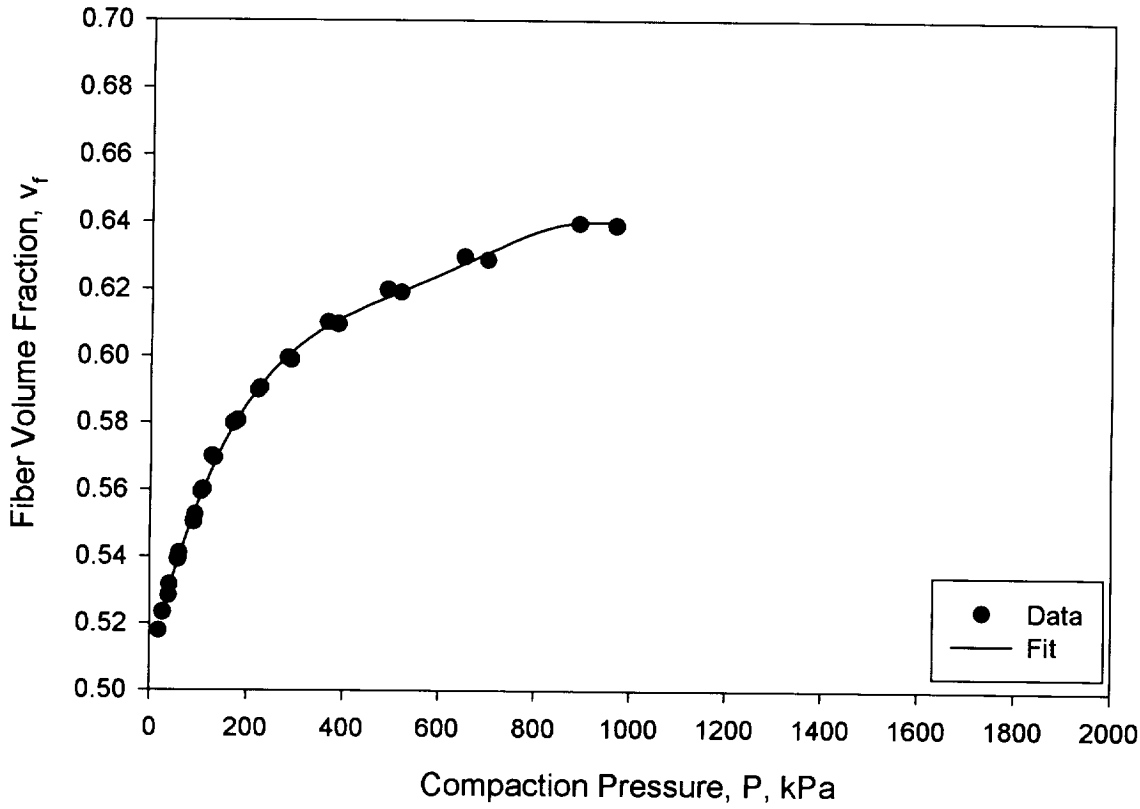

Figure 42: Compaction Behavior of Hexcel AS4 (0.3:1/8) Multiaxial Warp Knit Fabric.

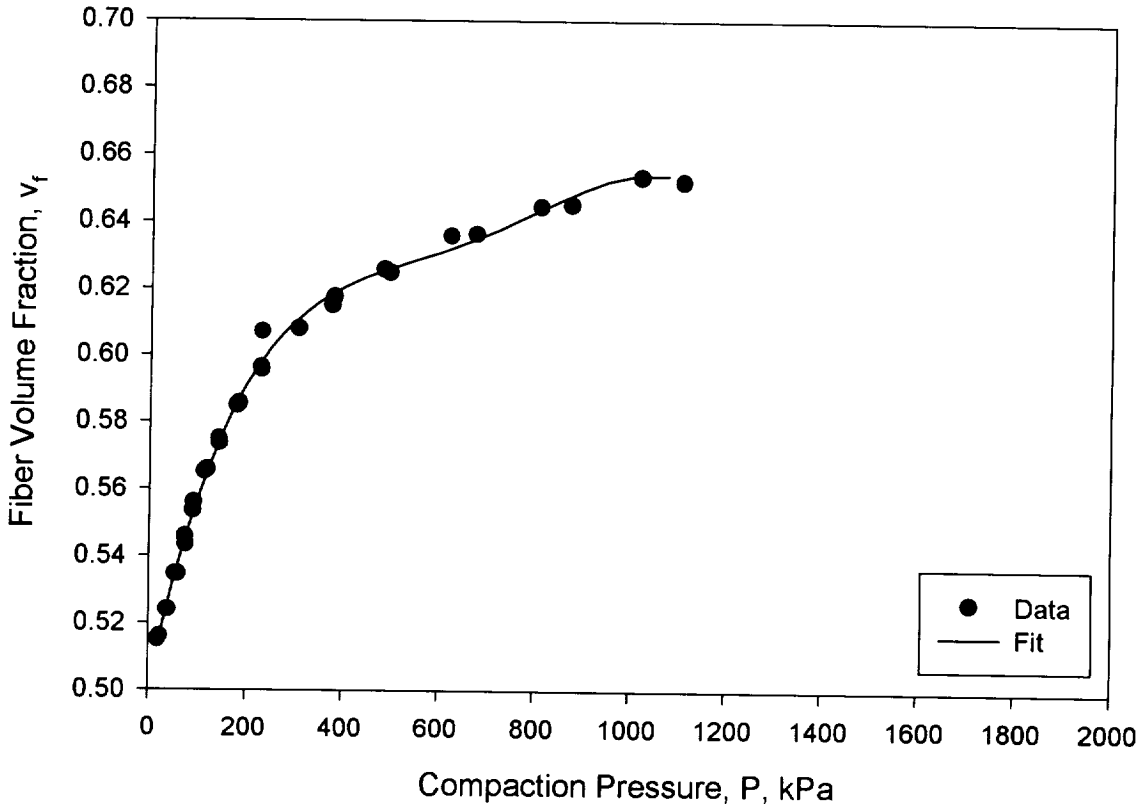

Figure 43: Compaction Behavior of Hexcel AS4 (0.5:1/8) Multiaxial Warp Knit Fabric.

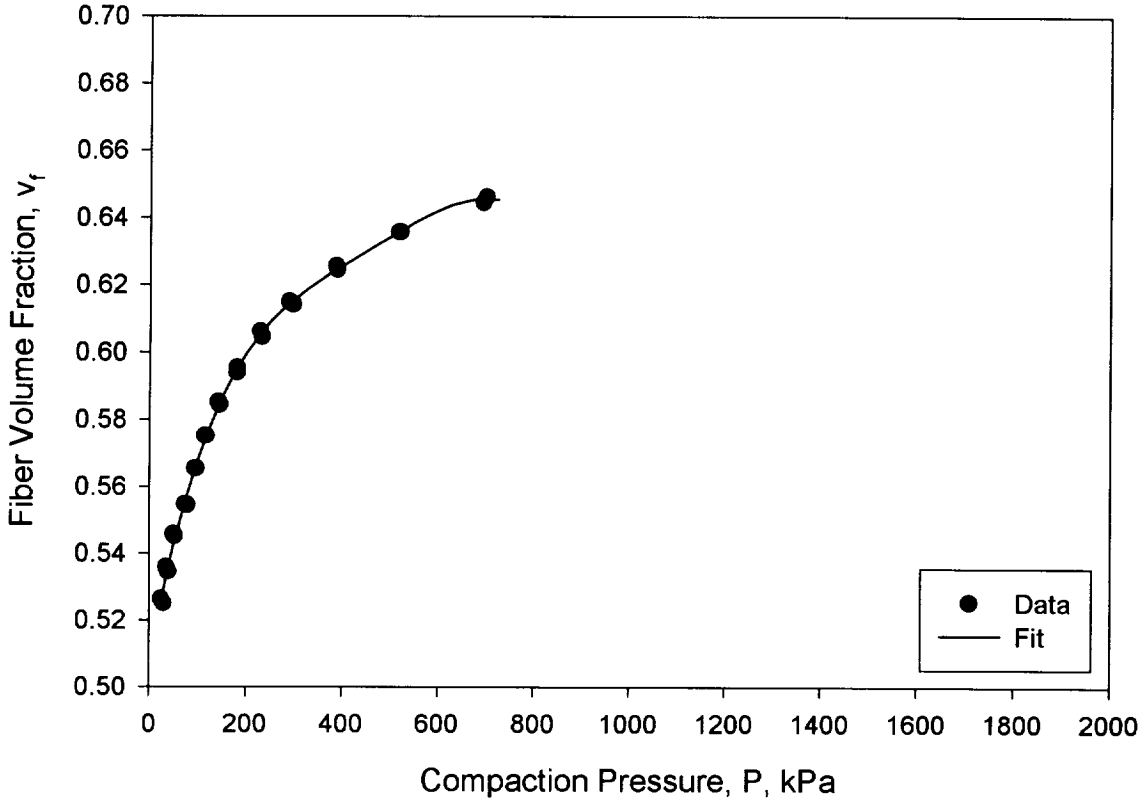

Figure 44: Compaction Behavior of Hexcel AS4 (0.75:1/8) Multiaxial Warp Knit Fabric.

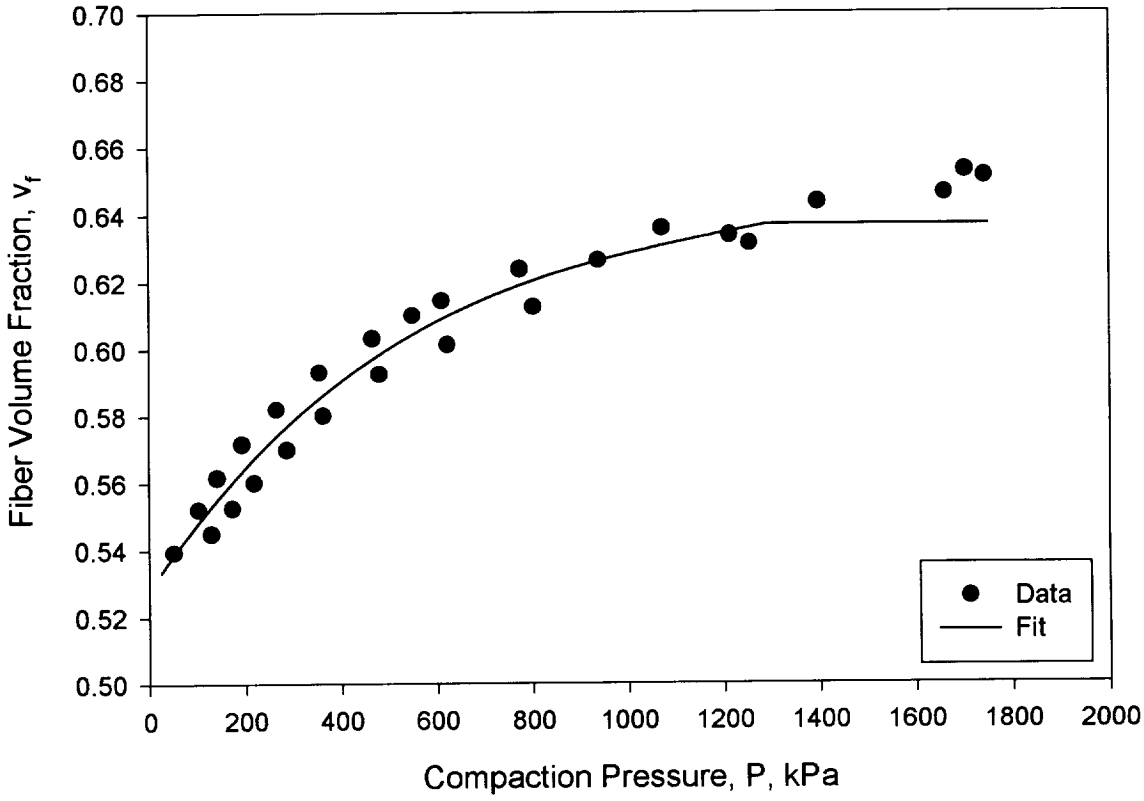

Figure 45: Compaction Behavior of Hexcel AS4/IM7 4 stack Multiaxial Warp Knit Fabric.

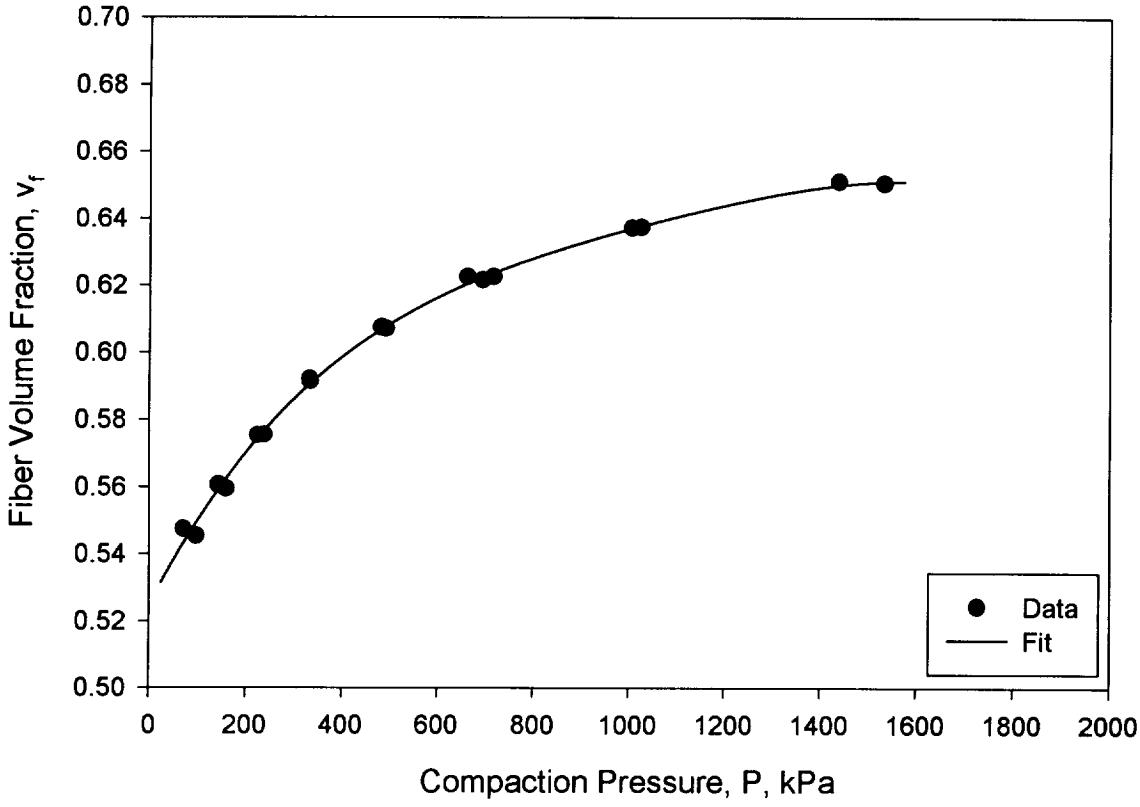

Figure 46: Compaction Behavior of Hexcel AS4/IM7 8 stack Batch 1 Multiaxial Warp Knit Fabric.

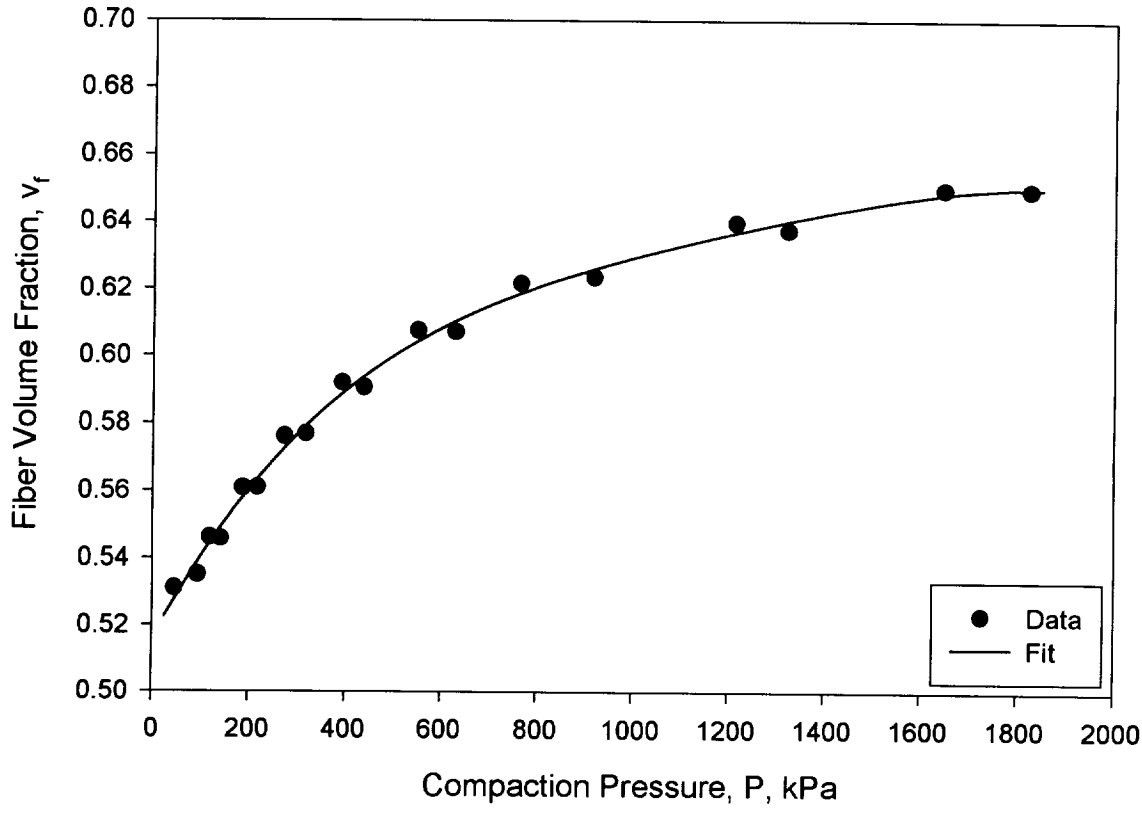

Figure 47: Compaction Behavior of Hexcel AS4/IM7 8 stack Batch 2 Multiaxial Warp Knit Fabric.

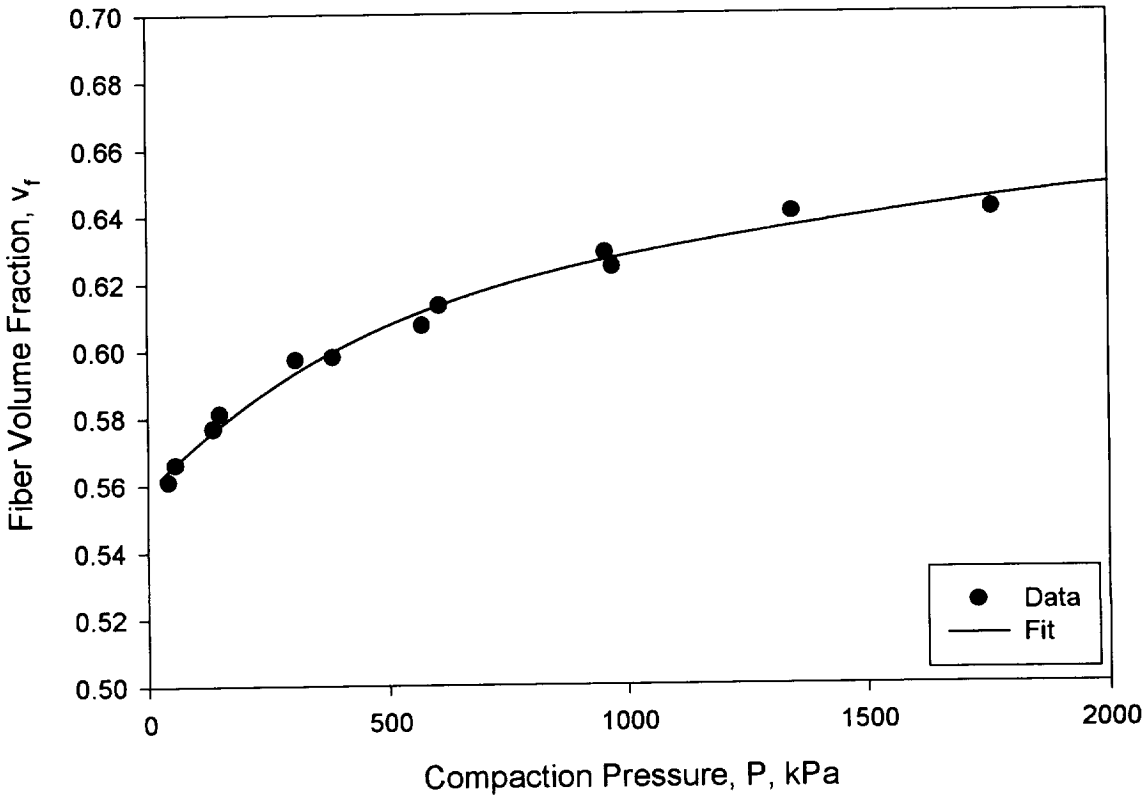

Figure 48: Compaction Behavior of Hexcel AS4/IM7 8 stack Heat Set Multiaxial Warp Knit Fabric.

Table 12: Fiber Volume Fraction Fit Constants for Various Materials.

	a_0	a_1 $\times 10^{-4}$	a_2 $\times 10^{-7}$	a_3 $\times 10^{-10}$	a_4 $\times 10^{-14}$	$\bar{\sigma}_{max}$ (kPa)
Tenax	0.50742	4.45047	-5.86561	3.57627	-8.12660	1515
AS4 (0.2:1/8)	0.52491	3.23476	-4.19359	2.79126	-7.11793	1450
AS4 (0.3:1/8)	0.50714	6.2558	-14.63388	16.6101	-69.41855	904
AS4 (0.5:1/8)	0.50065	7.05612	-15.61507	16.00585	-59.14343	1027
AS4 (0.75:1/8)	0.50734	8.07776	-23.32976	33.59910	-181.92638	687
AS4/IM7 4-stack	0.52808	2.13027	-16.55870	0.59082	-0.62061	1287
AS4/IM7 8-stack Batch 1	0.52457	2.83173	-3.11838	1.837829	-4.28921	1564
AS4/IM7 8-stack Batch 2	0.51584	2.70508	-2.66400	1.36598	-2.72584	1827
AS4/IM7 8-stack heat set	0.55870	1.44703	-1.88490	0.52077	-0.87847	2258
AS4/IM7 16-stack	0.55284	1.78598	-1.22525	0.26612	0.39585	1144
14-Tube Braid	0.55653	3.87254	-10.6127	15.6092	-82.2488	801
4-Tube Braid	0.52363	5.23703	-11.8842	13.6207	-57.6054	922
Knytex 7544 Glass	0.43599	2.17367	-1.46108	0.44764	-0.48617	3581
Boeing Glass 7544	0.41261	6.1959	-10.823	8.8075	-25.912	1288

The values of $a_0, a_1, \ldots, a_4$ for the materials tested are listed in Table 12. The fiber volume fraction is taken to be constant after a stress of $\bar{\sigma}_{max}$ is reached.

3.2 Compaction Results

The effect of stitch row spacing on compaction behavior was investigated using the AS4 MAWK stitched at (0.2:1/8), (0.3:1/8), (0.5:1/8), and (0.75:1/8). As can be seen in Figure 53 there is a visible trend in the fits to the compaction pressure vs. fiber volume fraction data as stitch density is varied. It is seen that as the stitch density decreases less compaction pressure is needed to produce the same fiber volume fraction.

The effect of preform thickness on compaction behavior was investigated in the Hexcel AS4/IM7 MAWK Fabric and the Triaxial Braid Fabric. Hexcel AS4/IM7 MAWK preforms with thicknesses of 4-stack, 8-stack, and 16-stack were tested. The fourth order polynomial fits to the compaction data for each thickness, shown in Figure 54, tend to indicate that as the preform thickness increases less compaction pressure is needed to produce a specific fiber volume fraction. It is noted that the 8-stack material behaves more like the 4-stack at

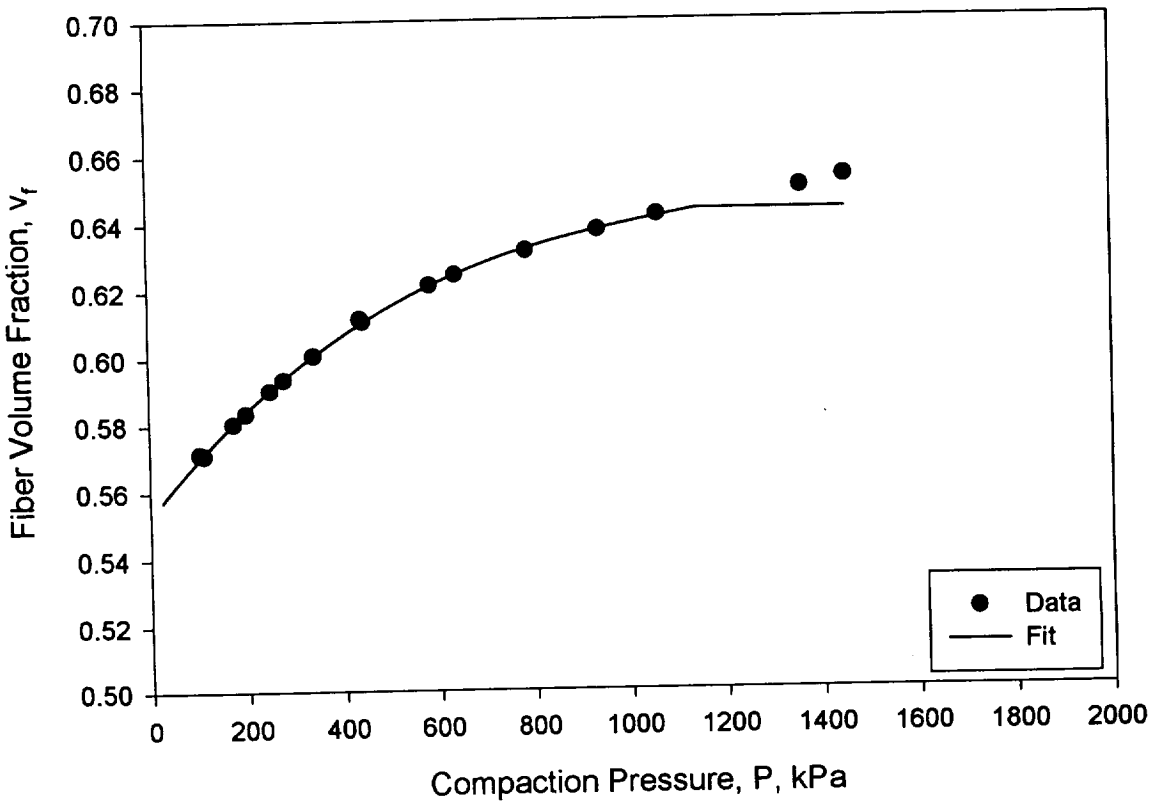

Figure 49: Compaction Behavior of Hexcel AS4/IM7 16 Stack Multiaxial Warp Knit Fabric.

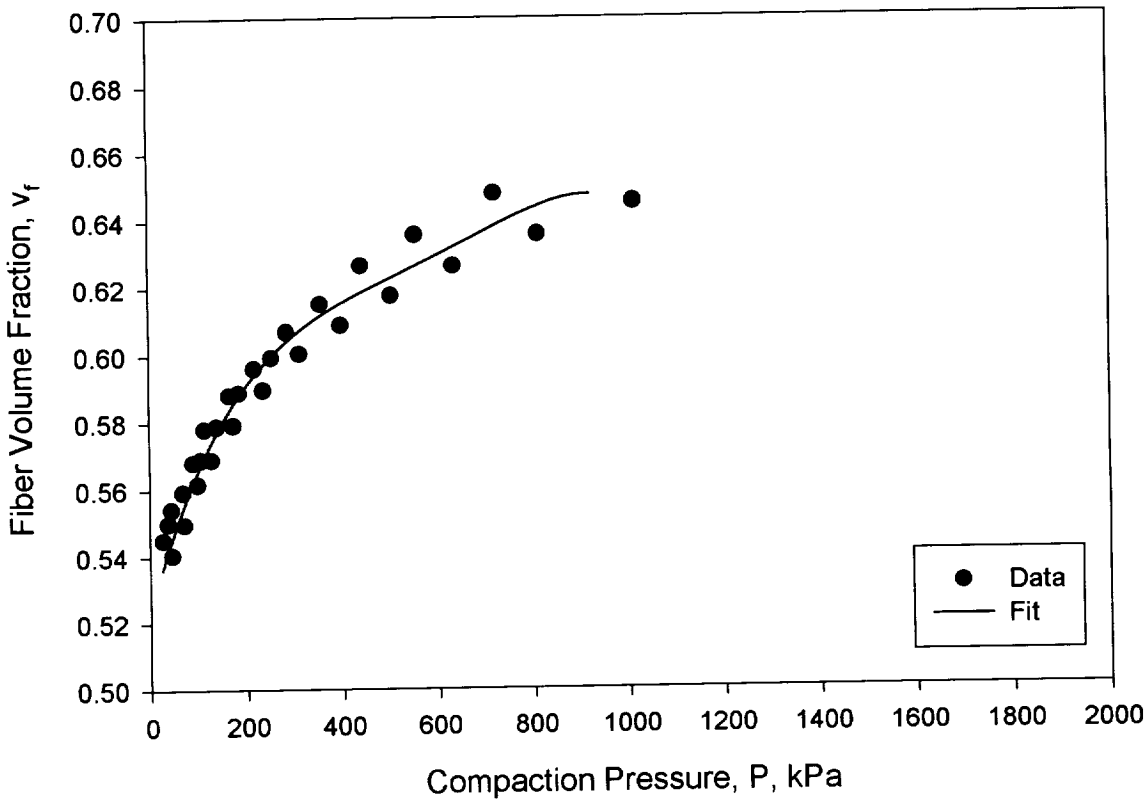

Figure 50: Compaction Behavior of 4-Tube Triaxial Braided Fabric.

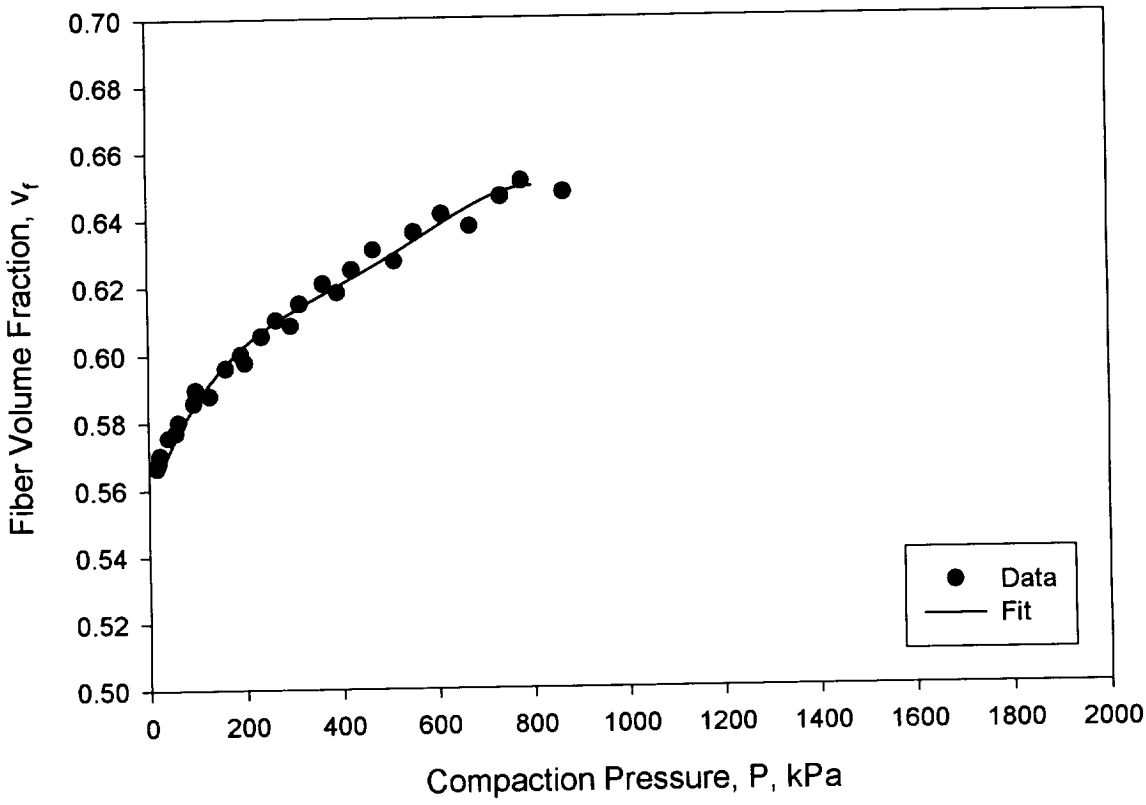

Figure 51: Compaction Behavior of 14-Tube Triaxial Braided Fabric.

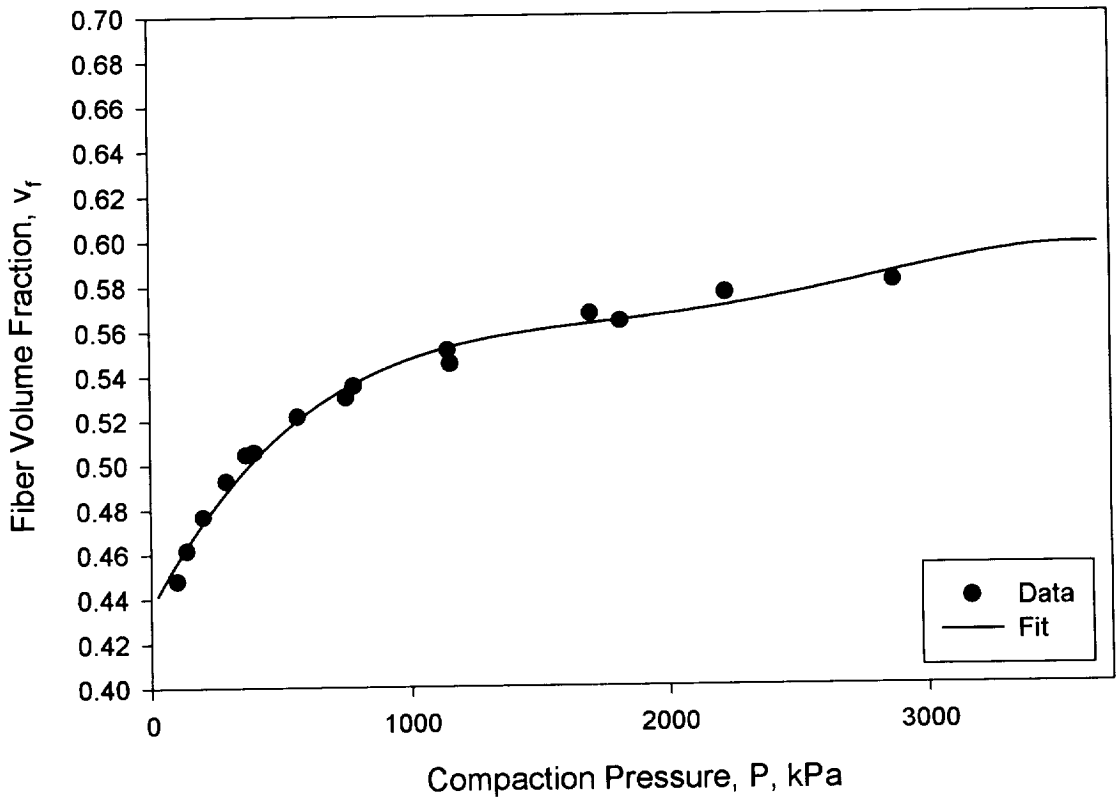

Figure 52: Compaction Behavior of Knytex 7544 Fabric (10 ply).

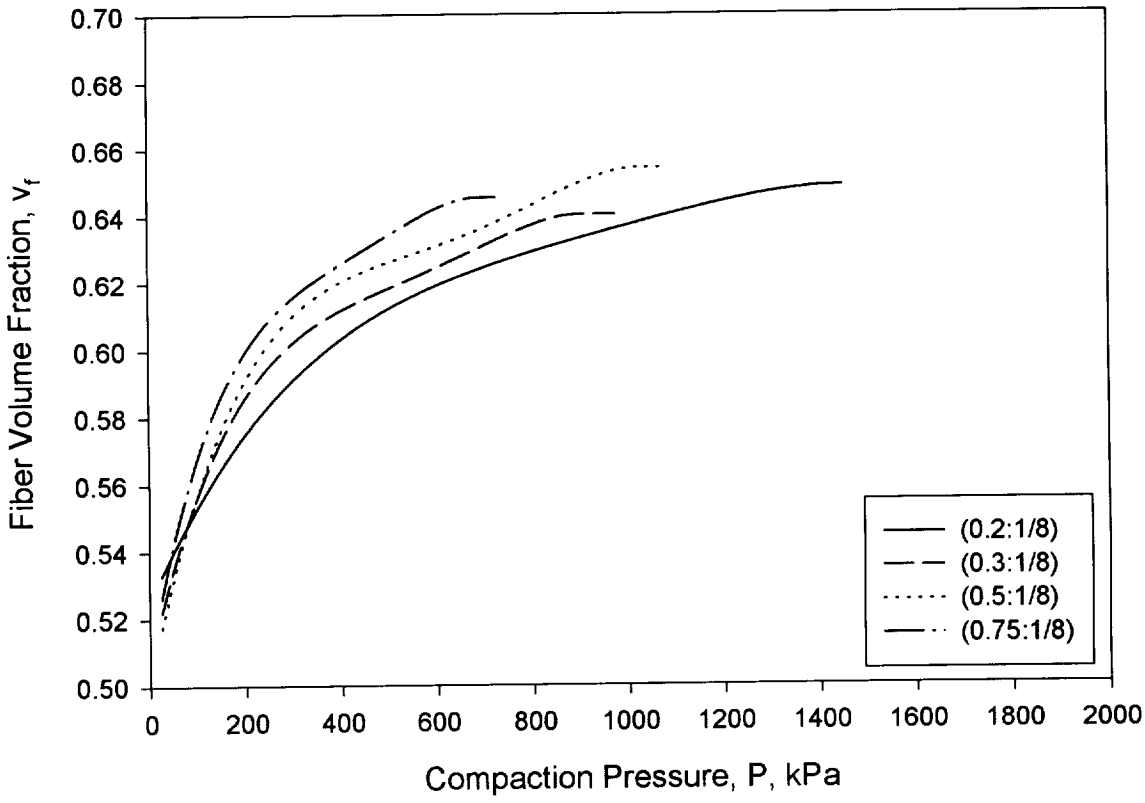

Figure 53: Effect of Stitch Density on Compaction in 6 stack Hexcel AS4 Preforms.

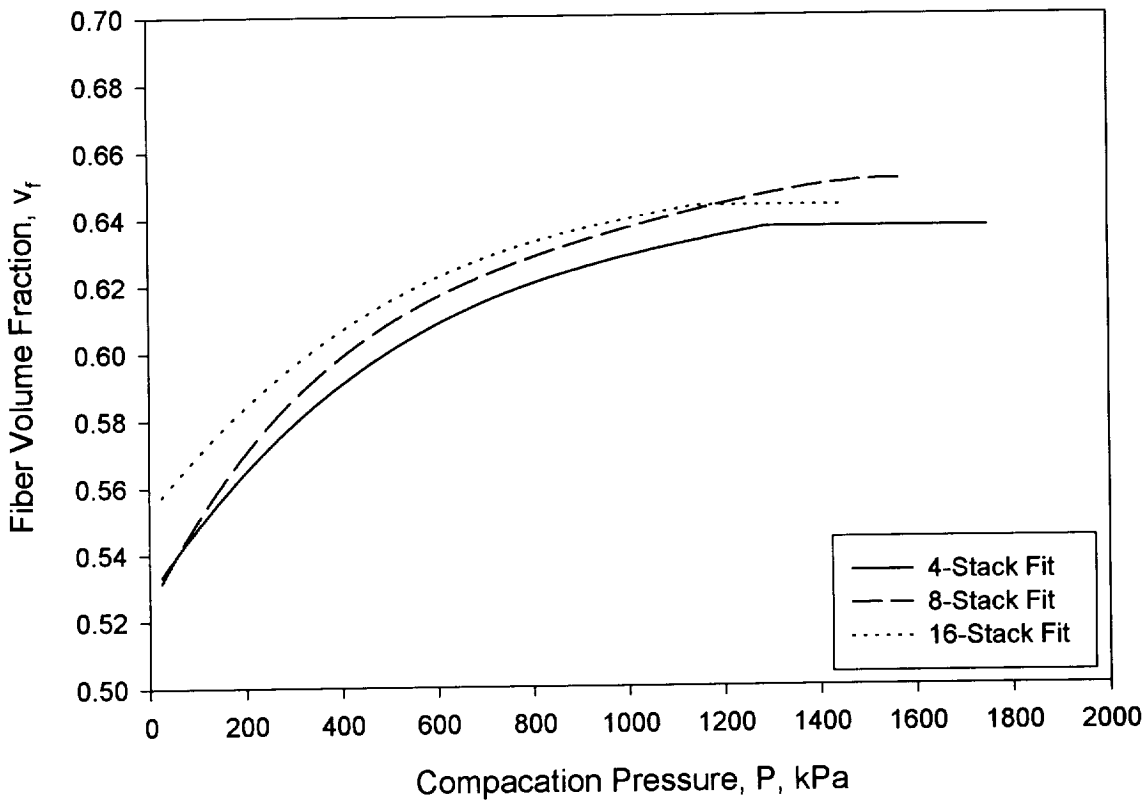

Figure 54: Effect of Thickness on Compaction in Hexcel AS4/IM7 Preforms.

low compaction pressures and more like the 16-stack at higher compaction pressures. The triaxial braid fabric was studied in two thicknesses, 4-tube and 14-tube. Figure 55 shows the polynomial fits to the data for the two thicknesses. Again as thickness increases less compaction pressure is required to produce a specific fiber volume fraction.

The effect of batch variability on compaction behavior was investigated by testing preforms from two batches of the 8-stack AS4/IM7 Multiaxial Warp Knit material. The variation in the data from the two batches and the polynomial fit to the data from the two batches is shown in Figure 56.

The effect of the heat set process on compaction behavior was also investigated. Several samples of the 8-stack AS4/IM7 MAWK from batch 2 were heat set prior to making compaction measurements. As seen in Figure 57 the heat set process does influence the compaction behavior of the preform. The heat set process compressed the preform so that those preforms that had been heat set started off with a higher initial fiber volume fraction.

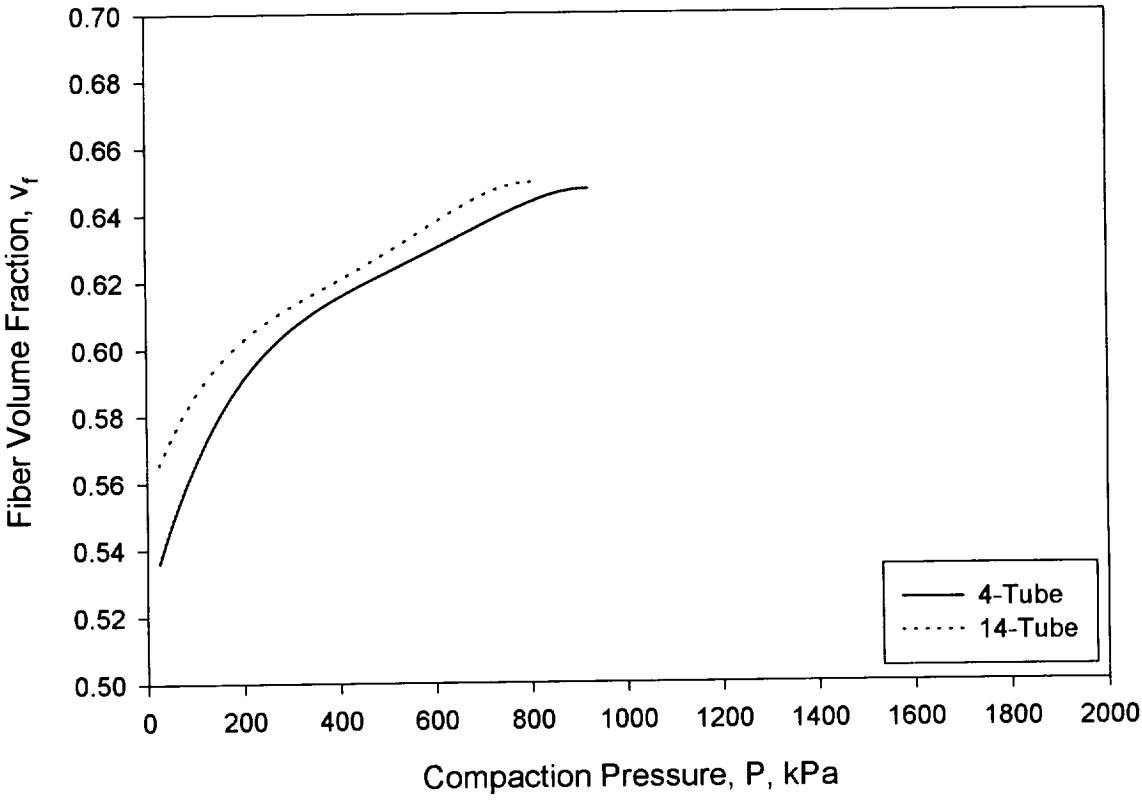

Figure 55: Effect of Thickness on Compaction in Trixial Braid Preforms.

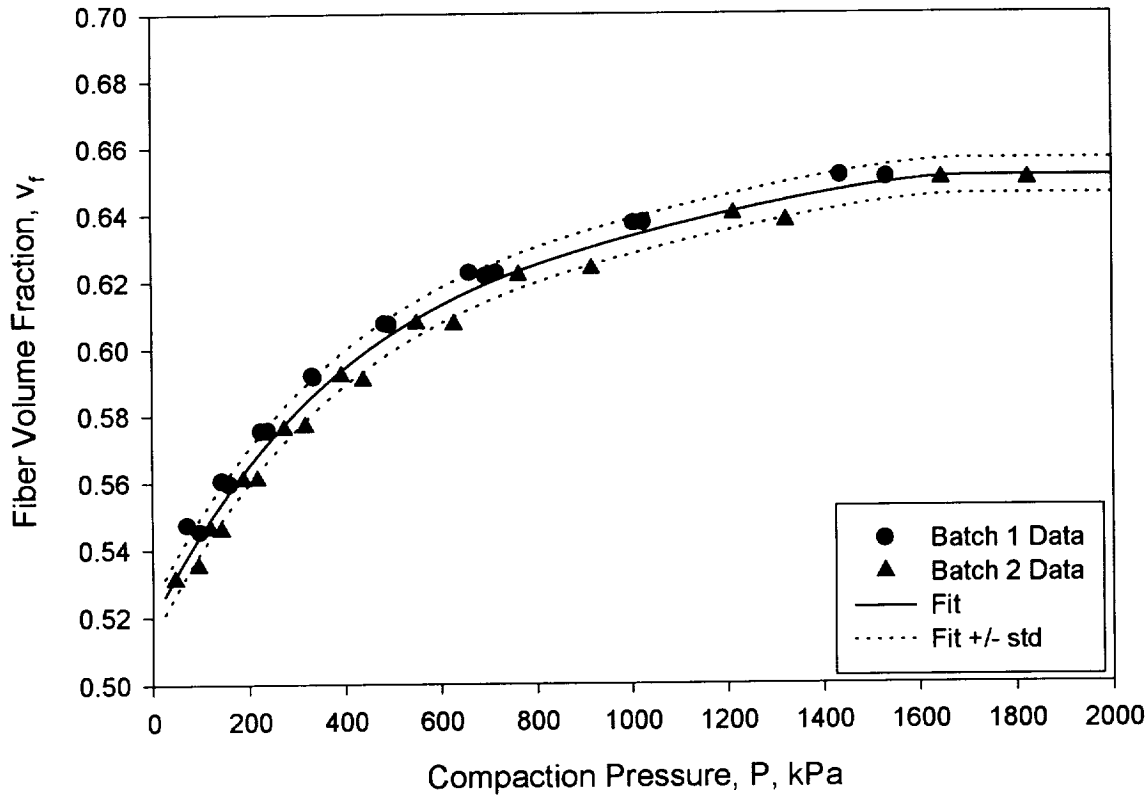

Figure 56: Effect of Batch Variability on Compaction in 8-stack Hexcel AS4/IM7 Preforms.

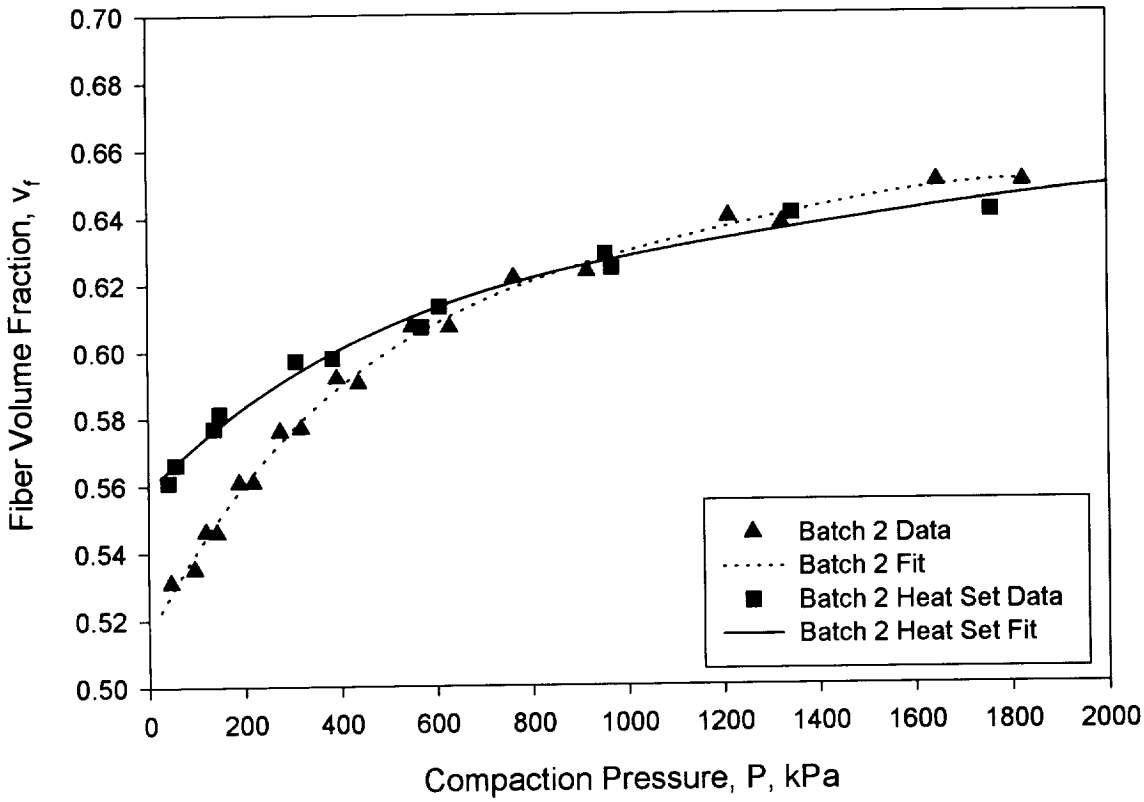

Figure 57: Effect of Heat Set Compaction in 8-stack Hexcel AS4/IM7 Preforms.

As fiber volume fractions reached 62 percent the effect of the heat set was reduced.

4 Summary

In this investigation a permeability measurement system for accurate, automated real-time measurement of fabric permeability was developed and used to measure the permeabilities or advanced fiber architecture preforms. Test fixtures to measure the compaction behavior and the in-plane and transverse permeabilities of textile preforms at high fiber volume fractions were developed. The test fixtures were successfully used to measure the compaction and permeabilities of advanced fiber architecture preforms to determine the effects of thickness, heat set, stitch density, and batch variablity.

The preforms tested were 8-stack Tenax MAWK, 6-stack AS4 MAWK, 4-, 8-, and 16-stack AS4/IM7 MAWK, and 4-tube and 14-tube braid. The Hexcel AS4 preforms were stitched at

several stitch densities. The stitch rows were spaced 0.2, 0.3, 0.5, or 0.75 inches apart, and the stitch step was 1/8 inch. The Tenax HTA and Hexcel AS4/IM7 preforms were stitched at 0.2 inch spacing and 1/8 inch step. The 8-stack AS4/IM7 was tested from two batches. In addition, some samples of the 8-stack AS4/IM7 were heat set prior to testing. Properties of the Knytex 7544 glass fabric were determined using 10 plys of the fabric stacked, but not stitched, together.

The in-plane and transverse permeabilities were measured for fiber volume fractions between 50 and 64 percent for graphite preforms and 45 and 60 percent for the glass fabric. Power-law curves were fit to the permeability versus fiber volume fraction data for use in the RFI simulation model.

Compaction measurements were performed to obtain a relation between the fiber volume fraction and the state of stress of the preform. Test data were taken at fiber volume fractions in the range of 50 to 64 percent. Fiber volume fraction versus effective stress (stress in the thickness direction of the material) were fit to a fourth order polynomial for use in the RFI model.

References

[1] Dexter, H. B., R. J. Palmer, and G. H. Hasko, "Mechanical Properties and Damage Tolerance of Multiaxial Warp Knit Structural Elements", in *Fourth NASA/DOD Advanced Composites Technology Conference, NASA CP-3229*, (June 7–11 1993).

[2] Hinrichs, S., R. J. Palmer, A. Ghumman, J. Deaton, K. W. Furrow, and L. C. Dickinson, "Mechanical Property Evaluation of Stitched/RFI Composites", in *Fifth NASA/DOD Advanced Composites Technology Conference, NASA CP-3294*, (August 22–25, 1994).

[3] Furrow, K. W., "Material Property Evaluation of Braided and Braided/Woven Wing Skin Blade Stiffeners", Contractor Report 198303, NASA, (April 1996).

[4] Fingerson, J. C., A. C. Loos, and H. B. Dexter, "Verification of a Three-Dimensional Resin Transfer Molding Prosess Simulation Model", Tech. Rep. CCMS-95-10, Virginia Tech Center for Composite Materials and Structures, (September 1995).

[5] Weideman, M. H., "An Infiltration/Cure Simulation Model for Manufacure of Fabric Composites by the Resin Infusion Process", Master's thesis, Virginia Polytechnic Institute and State University, (1992).

[6] Hammond, V. H., A. C. Loos, H. B. Dexter, and G. H. Hasko, "Verification of a Two-Dimensional Infiltration Model for the Resin Transfer Molding Prosess", Tech. Rep. CCMS-93-15, Virginia Tech Center for Composite Materials and Structures, (September 1993).

[7] Chamis, C., "Simplified Composite Micromechanics Equations for Hygral Thermal and Mechanical Properties", in *38th Annual Conference, The Society of Plastics Industry*, pp. Session 21C: 1–9, (February 1983).